

# The effect of water on Si and O diffusion rates in olivine and implications for transport properties and processes in the upper mantle

Fidel Costa<sup>a,b,\*</sup>, Sumit Chakraborty<sup>a,1</sup>

<sup>a</sup> Institut für Geologie, Mineralogie & Geophysik, Ruhr-Universität, Bochum, Bochum 44780, Germany

<sup>b</sup> CSIC, Institut de Ciències de la Terra 'Jaume Almera', Lluís Solé i Sabarís s/n, 08028 Barcelona, Spain

Received 27 April 2007; received in revised form 20 September 2007; accepted 15 October 2007

## Abstract

We performed piston cylinder experiments (1200–1350 °C, 2 GPa) to determine the diffusion rates of Si and O in mantle olivine under water undersaturated (brucite absent, 45 ppm H<sub>2</sub>O in olivine) as well as close to water-saturated (brucite present, ~370 ppm H<sub>2</sub>O in olivine) conditions. Diffusion couples consisted of oriented and polished San Carlos olivine cylinders coated with thin (~few 100 nm) films of the same composition enriched in <sup>29</sup>Si and <sup>18</sup>O, with a protective coating of ZrO<sub>2</sub> on top. Relationships between water solubility in olivine and water fugacity, combined with thermodynamic equilibrium calculations, indicate  $f\text{H}_2\text{O} \sim 1$  GPa,  $f\text{O}_2 \sim \text{IW}$  buffer for brucite absent and  $f\text{H}_2\text{O} \sim 9$  GPa,  $f\text{O}_2 \sim \text{QFM}$  buffer for brucite present experiments. We find that under hydrous conditions  $D_{\text{Si}} \approx D_{\text{O}}$  and diffusion anisotropy is weak to non-existent. Fitting the raw data at 2 GPa and  $f\text{H}_2\text{O} \sim 0.93$  GPa yields Arrhenius parameters [ $D_0$  and  $E_p$  in  $D = D_0 \exp(-E_p/RT)$ ] of:  $1.68 (\pm 3.52) \times 10^{-7} \text{ m}^2 \text{ s}^{-1}$  and  $358 \pm 28 \text{ kJ mol}^{-1}$  for Si, and  $1.43 (\pm 1.80) \times 10^{-4} \text{ m}^2 \text{ s}^{-1}$  and  $437 \pm 17 \text{ kJ mol}^{-1}$  for O, respectively (1 sigma errors).  $D$  (2 GPa,  $f\text{H}_2\text{O} = 0.97$  GPa, 1200 °C):  $D$  (1 atm., dry, 1200 °C) is 1000 for Si and 10 for O, respectively. Equations incorporating explicitly the effect of water are discussed in the text.

Analysis of our data suggests that O diffuses by an interstitial mechanism whereas Si diffuses via vacancy complexes. The relation between the water fugacity and the Si diffusion rates seems to obey a power law with a water fugacity exponent of 0.2–1. The amount of H incorporated into olivine at the experimental conditions is orders of magnitude higher than the likely concentration of Si vacancies. Therefore, a small fraction (~0.01%) of the total incorporated H in olivine suffices to considerably enhance the concentration of Si vacancies, and hence diffusion rates. Activation energies for O diffusion under dry and wet conditions are similar, indicating that the mechanism of this diffusion does not change in the presence of water. This inference is consistent with results of computer simulations.

Dislocation creep in olivine under wet conditions appears to be controlled by both, Si as well as O diffusion. Absolute creep rates can be calculated from the diffusion data if it is assumed that climb and glide of dislocations contribute equally to creep. Finally, analysis of the various transport properties indicate that <10 ppm of water in olivine is sufficient to cause a transition from “dry” to “wet” laws for most processes. As these water contents are even lower than the observed water contents in most mantle olivines (i.e. minimum values measured at the surface), we conclude that results of water present but undersaturated kinetic experiments are directly applicable to the mantle. Indeed, “wet” kinetic laws should be used for modeling geodynamic processes in the upper mantle, even if the mantle is thought to be undersaturated with respect to water.

© 2007 Elsevier B.V. All rights reserved.

**Keywords:** Diffusion; Water; Deformation; Olivine; Silicon; Oxygen; Creep; Mantle; Experiment; Nominally anhydrous mineral (NAM); Transport

## 1. Introduction

Water plays a crucial role in most biological, atmospheric, and surface geological processes. But it also has a large effect

on the physical properties of materials and processes that occur deeper within the Earth. Experimental results in the last two decades show that even small amounts (<0.005 wt.%) of H in nominally anhydrous minerals (NAMs) such as olivine or pyroxenes decreases the melting temperature and viscosity of the mantle, and enhances electrical conductivity and chemical diffusivity in it (e.g., Mei and Kohlstedt, 2000; Bolfan-Casanova, 2005; Hier-Majumder et al., 2005; Hirschmann, 2006; Karato, 2006; Yoshino et al., 2006; Wang et al., 2006; Demouchy et al., 2007). Despite the information that already exists, one can identify three main areas where more work is required:

\* Corresponding author at: CSIC, Institut de Ciències de la Terra 'Jaume Almera', Lluís Solé i Sabarís s/n, 08028 Barcelona, Spain.

Tel.: +34 93 4095410x265; fax: +34 93 4110012.

E-mail addresses: [fcosta@ija.csic.es](mailto:fcosta@ija.csic.es) (F. Costa), [Sumit.Chakraborty@rub.de](mailto:Sumit.Chakraborty@rub.de) (S. Chakraborty).

<sup>1</sup> Tel.: +49 234 322 4395; fax: +49 234 321 4433.

- (1) A robust quantification of the relation between the H content and the different physical properties at the relevant conditions does not exist. Measuring the rheological behavior of mantle material in the presence of water at upper mantle pressures remains a daunting challenge, with only two data sets obtained above 300 MPa (e.g., Hirth and Kohlstedt, 2003; Karato and Jung, 2003). However, precise relations between the “wet” vs. “dry” flow of these materials at high pressures are necessary to understand the factors that determine the nature of plate tectonics (e.g., Lithgow-Bertelloni and Richards, 1995; Hirth and Kohlstedt, 1996; Billen and Gurnis, 2001; Bercovici and Karato, 2003; Regenauer-Lieb, 2006).
- (2) The mechanistic connection between H incorporation and changes in the different transport properties such as ionic diffusion, deformation, and electrical conductivity remains unclear. Diffusion data in water-bearing olivine is limited to Fe–Mg (Hier-Majumder et al., 2005) and it is not directly related to deformation or electrical conductivity. Computer simulations (e.g., Brodholt and Refson, 2000; Walker et al., 2003; Wright, 2006), water solubility measurements (e.g., Bai and Kohlstedt, 1992; Kohlstedt et al., 1996; Keppler and Bolfan-Casanova, 2006), and spectroscopic studies of NAMs (e.g., Beran and Putnis, 1983; Beran and Libowitzky, 2006; Kohn, 2006) have contributed much to indicate the possible location of H in the olivine structure, but the results are far from conclusive.
- (3) It is necessary to quantify at what H concentration the physical and chemical behavior of mantle materials change from the dry to the water-bearing mechanisms/rates, and if such concentrations are likely to be present in the upper mantle. Studies of mantle xenoliths indicate that NAMs contain significant but very variable amounts of H (a few to a few hundred ppm; e.g., Bell and Rossman, 1992; Ingrin and Skogby, 2000). These water contents are typically lower than those at which the experimental data on physical properties are acquired. Nonetheless, evidence from modeling the mantle flow under the western U.S. seems to require a ‘wet’ rheological law (Dixon et al., 2004; Freed and Bürgmann, 2004).

Here we present experimental data on Si and O diffusion rates in mantle olivine in the presence of H, and use these results to

address some of the points above. We first explain in some detail the experimental and analytical strategy we have used. Next, the diffusion data are presented and the influence of the different intensive variables on the kinetic parameters are disentangled. The results are then discussed within the context of existing point defect thermodynamic models of olivine and related to Fe–Mg diffusion and dislocation creep rates of mantle olivine.

## 2. Experimental and analytical approach

One of the main challenges of the experiments was to ensure mechanical as well as chemical stability of olivine and of the diffusion couple (crystal plus thin film) during the water-bearing, high pressure and temperature annealing conditions. Thus, we describe below in some detail the problems encountered before reaching the final working configuration.

### 2.1. Starting materials and diffusion couples

San Carlos olivine crystals free of cracks or inclusions were selected and oriented parallel to one of the crystallographic axes using optical methods on a spindle stage. The orientations of some of these crystals were determined *a posteriori* using the EBSD technique (electron backscatter diffraction) on a scanning electron microscope and differences between the two methods were  $<10^\circ$ . The oriented crystals were cut into 1–2 mm thick slices and polished using diamond compounds followed by the combined mechano-chemical action of a highly alkaline colloidal silica solution (OP-S of Struers). We used cylinders that were drilled out of the olivine slices with a diameter of  $\sim 2.5$  mm and thickness of 1–2 mm.

The polished surfaces of the olivine cylinders were deposited with thin films (200–1000 nm thick) of the same olivine major element composition but doped with  $^{18}\text{O}$  and  $^{29}\text{Si}$  using the pulsed laser deposition facility available at the Institute of Geology, Mineralogy and Geophysics at Ruhr-Universität Bochum (Dohmen et al., 2002a, 2007). It was found that recrystallization, grain growth or dissolution during annealing destroyed the olivine thin film. This was overcome by depositing a second protective layer that would act inertly; after several tests a film of  $\text{ZrO}_2$  was found to be ideal for this purpose (Fig. 1a). Moreover, to minimize surficial effects and reaction with the environment, two such doubly coated crystals were placed on top of each other

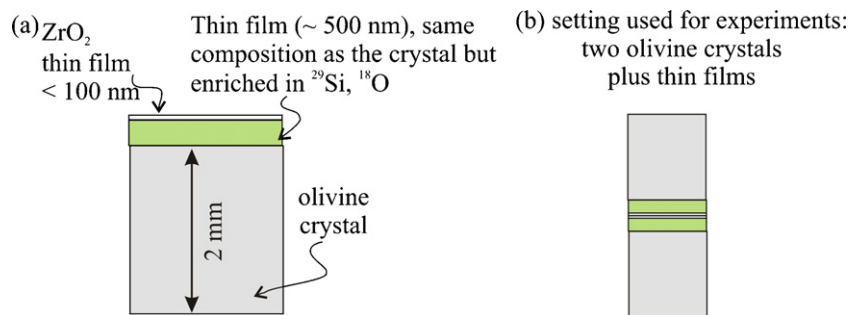


Fig. 1. (a) Olivine crystal plus thin films of olivine enriched in  $^{18}\text{O}$  and  $^{29}\text{Si}$  plus a protective thin film of  $\text{ZrO}_2$ . (b) A sandwich of two olivine crystals was used in the experiments. This setting prevented olivine thin films from reacting with the environment and yielded two crystals per anneal, providing a check for reproducibility of data.

Table 1  
Experimental conditions and diffusion coefficients determined in San Carlos Olivine (ca. Fo<sub>92</sub>)

|  | Orientation     | <i>T</i> (°C) | Time (h) | H <sub>2</sub> O ppm in olivine, measured | H <sub>2</sub> O ppm in olivine, calculated <sup>a</sup> | <i>f</i> H <sub>2</sub> O <sup>b</sup> (GPa) | Log <i>f</i> O <sub>2</sub> <sup>b</sup> (Pa) | <i>D</i> <sub>Si</sub> (m <sup>2</sup> s <sup>-1</sup> ) | <i>D</i> <sub>O</sub> (m <sup>2</sup> s <sup>-1</sup> ) | Observations                       |
|--|-----------------|---------------|----------|---|--|--|---|--|---|------------------------------------|
| ScOl25a  | Random          | 1350          | 6        |   | 51   | 0.89   | -5.8  | 9.91 × 10 <sup>-19</sup>                                 | 8.96 × 10 <sup>-19</sup>                                | Slow quench                        |
| ScOl25b  | Random          | 1350          | 6        |   | 51   | 0.89   | -5.8  | 6.99 × 10 <sup>-19</sup>                                 | 1.79 × 10 <sup>-18</sup>                                | Slow quench                        |
| scOl26a  | 23° with [00 1] | 1300          | 14       |   | 45   | 0.91   | -6.2  | 3.69 × 10 <sup>-19</sup>                                 | 6.73 × 10 <sup>-19</sup>                                | Slow quench                        |
| scOl26b  | 23° with [00 1] | 1300          | 14       |   | 45   | 0.91   | -6.2  | 3.35 × 10 <sup>-19</sup>                                 | 5.92 × 10 <sup>-19</sup>                                | Slow quench                        |
| ol4051b  | ⊥ [00 1]        | 1350          | 12       |   | 51   | 0.89   | -5.8  | 2.90 × 10 <sup>-19</sup>                                 | 1.07 × 10 <sup>-18</sup>                                | Slow quench                        |
| ol4051a  | ⊥ [00 1]        | 1350          | 12       |   | 51   | 0.89   | -5.8  | 2.30 × 10 <sup>-19</sup>                                 | 1.07 × 10 <sup>-18</sup>                                | Slow quench                        |
| ol4052a  | ⊥ [00 1]        | 1250          | 20       |   | 40   | 0.94   | -6.7  | 6.60 × 10 <sup>-20</sup>                                 | 2.07 × 10 <sup>-19</sup>                                | Slow quench                        |
| ol4041   | //[00 1]        | 1350          | 12       | 29  | 51   | 0.89   | -5.8  | 2.30 × 10 <sup>-19</sup>                                 | 1.01 × 10 <sup>-18</sup>                                | Slow quench                        |
| ol4042   | //[00 1]        | 1250          | 20       | 19  | 40   | 0.94   | -6.7  | 7.50 × 10 <sup>-20</sup>                                 | 9.20 × 10 <sup>-20</sup>                                | Slow quench                        |
| olF1-1   | //[00 1]        | 1275          | 20       | 16  | 43   | 0.93   | -6.5  | 1.18 × 10 <sup>-19</sup>                                 | 1.77 × 10 <sup>-19</sup>                                | Slow quench                        |
| olF1-1b  | //[00 1]        | 1275          | 20       | 16  | 43   | 0.93   | -6.5  | 1.57 × 10 <sup>-19</sup>                                 | 2.48 × 10 <sup>-19</sup>                                | Slow quench                        |
| OLF1-3   | //[00 1]        | 1200          | 48       |   | 35   | 0.97   | -7.2  | 2.68 × 10 <sup>-20</sup>                                 | 4.19 × 10 <sup>-20</sup>                                | Slow quench                        |
| ol40f14_2a1  | //[00 1]        | 1200          | 48       |   | >370   | >9.4   | ca. -3.9                                      | 5.37 × 10 <sup>-20</sup>                                 |   | Slow quench,<br>brucite<br>present |
| ol40f14_2a2  | //[00 1]        | 1200          | 48       |   | >370   | >9.4   | ca. -3.9                                      | 7.52 × 10 <sup>-20</sup>                                 |   | Slow quench,<br>brucite<br>present |
| ol40f14_2b1  | //[00 1]        | 1200          | 48       |   | >370   | >9.4   | ca. -3.9                                      | 4.29 × 10 <sup>-20</sup>                                 |   | Slow quench,<br>brucite<br>present |
| ol40f12_3a1  | //[00 1]        | 1300          | 20       | 11  | 45   | 0.91   | -6.2  | 4.10 × 10 <sup>-19</sup>                                 | 5.39 × 10 <sup>-19</sup>                                | Slow quench                        |
| ol40f13_1a1  | //[00 1]        | 1225          | 64       | 19  | 37   | 0.95   | -7.0  | 5.96 × 10 <sup>-20</sup>                                 |   | Slow quench                        |
| ol40f13_1b1  | //[00 1]        | 1225          | 64       | 19  | 37   | 0.95   | -7.0  | 5.96 × 10 <sup>-20</sup>                                 |   | Slow quench                        |
| ol40f13_2a1  | //[00 1]        | 1325          | 16       | 13  | 48   | 0.90   | -6.0  | 6.63 × 10 <sup>-19</sup>                                 |   | Slow quench                        |
| ol40f13_2a2  | //[00 1]        | 1325          | 16       | 13  | 48   | 0.90   | -6.0  | 7.89 × 10 <sup>-19</sup>                                 |   | Slow quench                        |
| ol40f11_3a1si  | //[00 1]        | 1300          | 14       |   | 45   | 0.91   | -6.2  | 1.17 × 10 <sup>-19</sup>                                 |   | Slow quench                        |
| ol40f11-2a1  | //[00 1]        | 1325          | 5        |   | 48   | 0.90   | -6.0  | 1.58 × 10 <sup>-19</sup>                                 |   | Slow quench                        |
| Experiments to quantify the water contents present at run conditions |                 |               |          |   |  |  |   |  |   |                                    |
| 14F_1  | //[00 1]        | 1275          | 20       | 43  |  | 0.93 <sup>c</sup>                            | -6.6  |  |   | Fast quench                        |
| 40F2TR   | //[00 1]        | 1250          | 20       | 40  |  | 0.94 <sup>c</sup>                            | -6.7  |  |   | Fast quench                        |
| 14F_5B   | //[00 1]        | 1225          | 40       | 370                                       |  | 9.4 <sup>c</sup>                             | ca. -3.9                                      |  |   | Fast quench,<br>brucite<br>present |

All experiments at 2 GPa. (//) Parallel to an axis; (⊥) perpendicular to an axis.

<sup>a</sup> Water content in the olivine calculated from water solubility equation of Zhao et al. (2004) and the fugacity obtained from fluid equilibria modeling results. For the samples with the highest *f*H<sub>2</sub>O, the *f*O<sub>2</sub> was calculated from an *f*H<sub>2</sub>O of 9.2 GPa because this is the maximum possible value that can be obtained using the presence of graphite and the equations of state for fluids mentioned in the text. It is worth noting that the fugacity of pure water from the EOS of Pitzer and Sterner (1994) used in the Zhao et al. (2004) calibration are about 5% higher (at the investigated *P* and *T*) than that of Holloway (1981).

<sup>b</sup> Water and oxygen fugacities calculated using the fluid composition of quickly quenched samples as obtained from modeling their C–O–H fluid equilibria.

<sup>c</sup> Water fugacity calculated using the measured OH concentration in olivine and the solubility equation of Zhao et al. (2004).

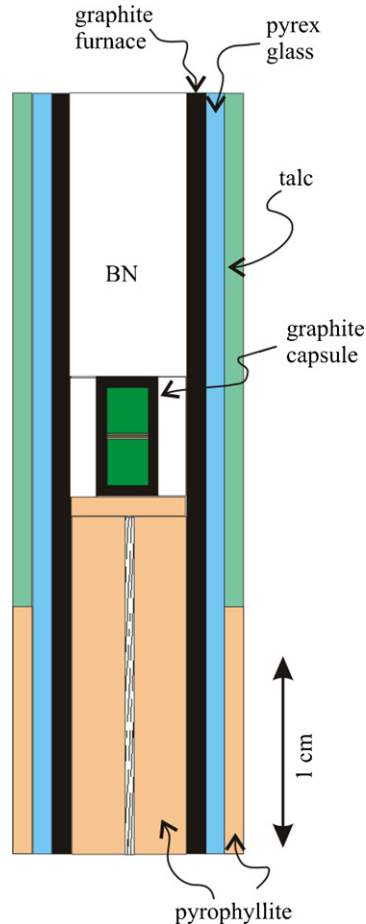


Fig. 2. Sketch of cell assembly used in the piston-cylinder experiments.

in a “sandwich” geometry (Fig. 1b). With this approach we also obtained two olivine crystals from each experiment in which diffusion profiles could be measured, and this provided a check of the internal consistency and reproducibility of data.

## 2.2. Experimental techniques

All experiments were performed in an end-loaded piston cylinder. The observed pressure was found to be within 0.2 GPa of the quartz-coesite transition reported by Bose and Ganguly (1995a). Temperatures were monitored using a  $W_{25}$ – $Re_{75}$  thermocouple and no pressure correction was made to the thermocouple readings. All experiments were performed at 2 GPa and over a temperature range of 1200–1350 °C at 25 °C intervals (Table 1).

The cell assembly (Fig. 2) is similar to other high pressure diffusion experiments in the piston cylinder (Elphick et al., 1985; Chakraborty and Ganguly, 1992). The main problems that we encountered were to find an assembly that was soft and unreactive with the olivine and thin film under water-present conditions. We tested several capsule materials including, NaCl, Ni, Mo, and  $Au_{75}Pd_{25}$ , since these were successful in previous experiments (e.g., Goldsmith, 1991; Graham and Elphick, 1991; Chakraborty and Rubie, 1996; Kohlstedt et al., 1996; Pichavant et al., 2002). It was found that NaCl corroded the olivine sur-

face, whereas the Ni, Mo and  $AuPd$  were not soft enough and the crystals were recovered completely crushed. To try to overcome this we surrounded the crystals with brucite and talc as in the set up used in the water solubility in olivine experiments of Kohlstedt et al. (1996). However, contrary to the observations of Kohlstedt et al. (1996) at lower temperatures ( $\sim 1100$  °C), many of our crystals completely reacted with the surroundings due to the higher temperatures that we need to induce significant diffusion (1200–1350 °C). In the experiments where  $Au_{75}Pd_{25}$  capsules were in direct contact with the olivine it was found using Rutherford Backscatter Spectroscopy (RBS) that the crystal had changed its composition within the first few tens of nm of its surface (the region of our interest) due to Fe loss to the capsule. Thus, although for many purposes Fe loss with this type of material is negligible (e.g., Pichavant et al., 2002) it is not the case when studying concentration differences at the nanometer scale.

Finally, two capsule setups were successful. The crystals were set in a graphite matrix and graphite capsule, or they were set in a graphite inner capsule surrounded by a brucite powder and this was enclosed in a welded  $Au_{75}Pd_{25}$  outer capsule. Using these setups we were able to recover undamaged single crystals of olivine, but the pressure and temperature range that can be investigated is limited by the stability of orthopyroxene + magnesite relative to olivine + graphite. SEM images of some early runs (Fig. 3) clearly demonstrate the consequences of crossing this reaction boundary. In most experiments we did not explicitly add water, but these nominally “dry” runs were found to be water-bearing, and the source of water was the talc of the cell assembly (Fig. 2). In some experiments we added brucite as a source of water. Brucite breaks down to MgO and water at run conditions (e.g., Johnson and Walker, 1993) and if the capsule remains closed, the breakdown products recombine to form brucite during cooling because MgO is non-quenchable in the presence of water. We performed X-ray diffraction of the powder from brucite present runs after annealing to ensure that the diffusion data that we report are from runs with excess water (i.e. olivine is H saturated).

A final requirement to prevent breaking of the crystals was to use pressure and temperature ramps (of ca. 30 min each) to start and end the experiments (e.g., Tingle, 1988). In experiments carried out in this manner only few cracks formed in the crystals and those that did form were perpendicular to the length of the cylinder so that the polished surface was still available for analysis. However, such a slow cooling and decompression path combined with the high diffusivity of H (Mackwell and Kohlstedt, 1990; Kohlstedt and Mackwell, 1998, 1999; Demouchy and Mackwell, 2003, 2006) allows it to leave the olivine crystals. Thus, the measured water contents after annealing underestimates the actual concentration present in the olivine during the runs. Note that where we write ‘water content in the olivine’ we do not imply molecular water present in the crystal but we refer to the H recalculated as  $H_2O$ . The magnitude of this degassing effect was established by performing three additional experiments at 2 GPa and two selected temperatures (1200 and 1225 °C). These runs were quenched in less than 1 min to retain the H contents in olivines from close to the annealing conditions. Inspection of these quickly quenched crystals with

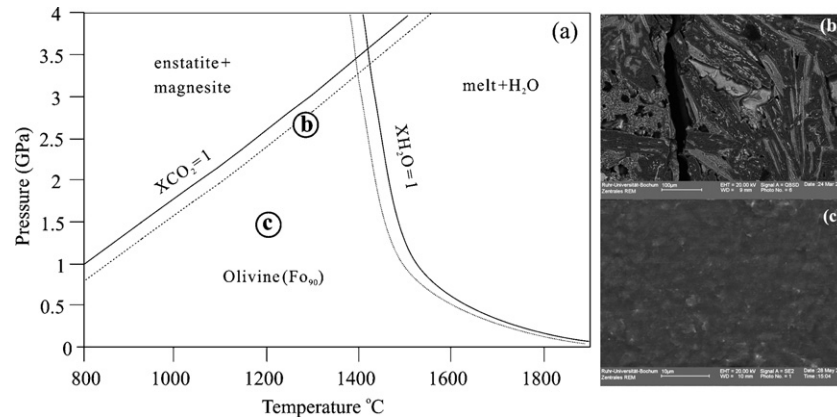


Fig. 3. (a) Breakdown of olivine to orthopyroxene and magnesite or melting of olivine in the presence of high water content limit the ranges of  $P$ – $T$  over which experiments can be carried out. Solid lines are for pure forsterite, and dotted lines are estimated positions for  $\text{Fo}_{90}$ . The pressure–temperature conditions of two experiments are marked as circles and textures observed on the respective run products are shown in (b) and (c) parts of the figure. (b) SEM image of olivine surface after high- $P$  and  $T$  annealing [precise conditions shown in (a)]. One can see a reaction texture where olivine is transformed to orthopyroxene (light grey) and magnesite (dark grey). (c) Surface of the olivine after annealing within its stability field [lower  $P$  and  $T$ , see circle in (a)]. The thin film looks like a fine-grained recrystallized material appropriate for determining diffusion data (e.g., Dohmen et al., 2002a, 2007).

the optical microscope shows that they contain numerous crystallographically oriented polyphasic inclusions with bubble(s) and some unidentified transparent and opaque material (Fig. 4). These inclusions were formed by the precipitation and nucleation of water during the fast quench (Mackwell et al., 1985; Karato, 2006), because such inclusions were not seen in the slowly quenched run products. During slow quench, excess H was able to escape from the crystal by diffusion without precipitating inclusions. Although the crystals from the quickly quenched runs cannot be used for the determination of diffusion coefficients (because as we note above, they break into multiple pieces) we consider their OH concentrations to be representative of those that prevailed in the crystals from which we obtained the diffusion data. We have used a sequence of calculations to obtain the water contents at annealing conditions, and based on that, fugacities of volatile species at run conditions for all crystals (see Section 3.3).

Uncertainties related to the thermocouple calibration and pressure correction of the emf reading are  $<0.5\%$  (Mao et al., 1971). The main temperature uncertainty in piston cylinder experiments is related to the presence of gradients in the furnace or the position of the thermocouple and the crystals. Using the thermal analysis of Watson et al. (2002) we estimate that

at our runs conditions and sample size (ca. 4 mm) temperature gradients are  $<20^\circ\text{C}$ , and thus we have adopted a conservative temperature uncertainty of  $\pm 10^\circ\text{C}$ .

### 2.3. SIMS analyses of olivine diffusion profiles

After the anneals, single crystals were recovered and mounted in indium/epoxy for ion microprobe analysis. Isotopic profiles were measured by secondary ion mass spectrometry (SIMS) using a Cameca IMS 4f ion probe (University of Edinburgh, UK). A primary Cs-ion beam (10–20 nA) was accelerated at 10 kV on to the Au-coated samples. High energy (300 eV) negative secondary ions were detected using an electron multiplier. The Si and O isotopes were measured simultaneously ( $^{16}\text{O}$ ,  $^{18}\text{O}$ ,  $^{28}\text{Si}$ ,  $^{29}\text{Si}$ ,  $^{30}\text{Si}$ ) and thus the position of the interface could be inferred from profiles of both the elements, and diffusion rates of the two elements could be studied in direct comparison. The depth of the profiles varied between 300 and 2700 nm and the sizes of the craters were about  $100\ \mu\text{m} \times 100\ \mu\text{m}$ . In total, 52 ion microprobe isotope profiles have been obtained—35 through annealed crystals and 17 in unannealed crystals which were used for checking the composition and shapes of the diffusion couples prior to experiments (i.e. initial conditions). Only 15 profiles

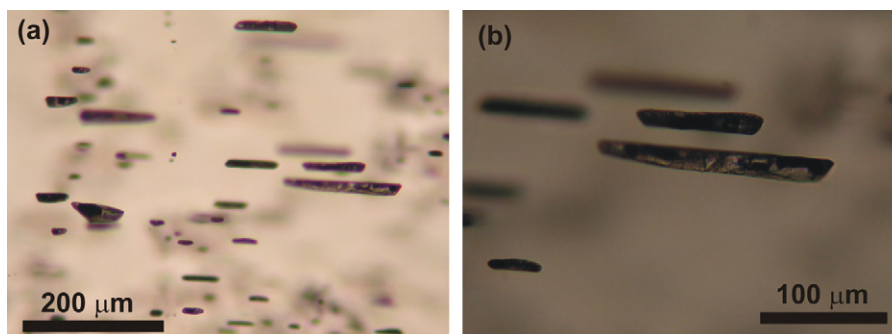


Fig. 4. Photomicrographs of olivine crystal annealed at 2 GPa,  $1225^\circ\text{C}$  and with excess water present. This crystal was quickly (ca. 1 min) quenched from run to near ambient conditions. It shows polyphase crystallographically oriented inclusions made of opaque phases and bubbles, Sample 40F2TR. These inclusions are not present in the slowly quenched runs.

have been finally used to obtain diffusion coefficients, the rest being discarded due to problems mainly related to the roughness of the sample surface. The lengths of the profiles were calibrated by measuring the depths of the individual sputter pits using a profilometer. Typically, measurements were carried out in four different directions for each crater and the crater morphology was also inspected to avoid artefacts. The experimental setup discussed above allows two crystals to be recovered from each run, allowing two determinations of diffusion coefficients from each experiment. The convolution lengths (i.e., length of the transition zones) of unannealed crystals range from 10 to 45 nm, whereas the lengths of the diffusion zones of the annealed crystals ranged from about 200 to 700 nm. This means that convolution effects were minimal, with a maximum possible 10% overestimation of the diffusion coefficients (Ganguly et al., 1988).

#### 2.4. Fourier transform infrared analysis of olivine

After the anneal and in some cases after the ion microprobe analyses the crystals were doubly polished and OH contents were determined by Fourier Transform Infrared spectroscopy (FTIR). The spectra were obtained from oriented crystals and a polarized beam of ca. 100  $\mu\text{m}$  in diameter at the Bayerisches Geoinstitut (Germany) with a Bruker IFS 120 high-resolution FTIR spectrometer. Spectra were obtained in two perpendicular directions (parallel to the  $a$  and  $b$  axes) for each crystal. A tungsten light source, a Si-coated  $\text{CaF}_2$  beam splitter and a narrow-band MCT detector were used for all measurements. Polarized measurements were carried out with an Al wire strip polarizer on a KRS-5 substrate. During the measurements, the interferometer chamber was kept under vacuum while the microscope was purged with purified air. Two hundred scans were measured at 4  $\text{cm}^{-1}$  resolution. The spot size analyzed was determined by an aperture in the rear focal plane of the 15-fold Cassegranian objective.

### 3. H loss, interpretation of FTIR spectra, and $f\text{H}_2\text{O}$ and $f\text{O}_2$ of the experiments

Understanding the effect of water on ionic diffusion rates and mechanism depends critically on our ability to determine the water fugacity of the experimental runs, and possibly also the oxygen fugacity. This is not straightforward because the  $f\text{H}_2\text{O}$  and  $f\text{O}_2$  cannot be directly controlled in high  $P$ – $T$  anneals in piston cylinder experiments. Constraining  $f\text{H}_2\text{O}$  and  $f\text{O}_2$  typically requires thermodynamic calculations combined with H determinations after anneals. In this section we address in some detail the problem of H loss during quench, the interpretation of the FTIR spectra of olivine, and how we obtain the volatile fugacities ambient during the anneals.

#### 3.1. The case of H loss during quenching

We have explored the extent of H loss from the olivines during quenching of the anneals by a series of numerical experiments. The temperature–pressure–time ( $T$ – $P$ – $t$ ) paths of experiments were recorded by the computer which controls the

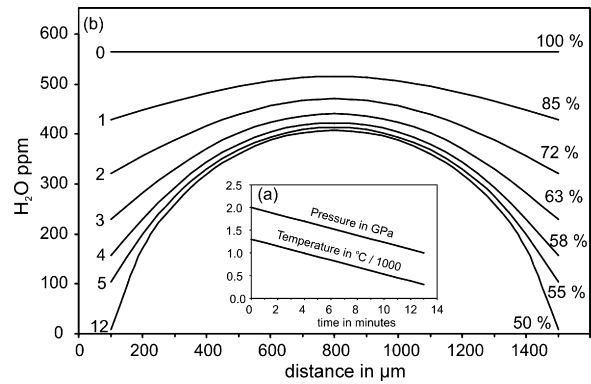


Fig. 5. A typical experiment took about 30 min to go from the high- $P$  and  $-T$  conditions to near room  $P$ ,  $T$  and the paths (80–90 °C and 0.07 GPa per minute, respectively) are shown in (a). We have modeled the effect of such a  $P$ – $T$ – $t$  path on the water content of the olivine by incorporating the  $T$  dependence of the diffusion coefficient of H from Kohlstedt and Mackwell (1998) in a diffusion model with a changing boundary condition according to the  $T$  and  $P$  dependence of the water fugacity using the equation of state of Pitzer and Sterner (1994) and the solubility model of Zhao et al. (2004). Thus the water content at the boundary is the maximum allowed solubility at a given  $P$  and  $T$  in the presence of a pure water fluid. (b) Model calculations of diffusive reequilibration in one dimension for a 1.5 mm thick slab using the diffusion data parallel to  $a$  axis. Numbers on the left of the calculated profiles are the times in minutes and numbers on the right are the amount of water (averaged through the crystal expressed in % with respect to the starting value) that remains. It is apparent that with the  $P$ – $T$ – $t$  paths we used in our experiments and which were required to retrieve crystals in good physical condition to be analyzed for diffusion, crystals can lose up to 50% of their water content. Such a change is consistent with the difference in total water contents analyzed by FTIR from quickly and slowly quenched runs (Table 1).

piston cylinder experimental apparatus. One dimensional diffusion calculations were carried out to model diffusion along these  $T$ – $P$ – $t$  paths, and the results show that (Fig. 5) already during the first 5 min of decompression and cooling as much as 50% of H is lost. This is similar to the difference between the water contents of olivines from slowly and fast quenched runs, and suggests that the low H content of olivines in the slowly quenched runs are due to diffusional H loss; these samples were not annealed with such low H contents.

#### 3.2. FTIR spectra of olivines in the region 3100–3800 $\text{cm}^{-1}$ and quantification of $\text{H}_2\text{O}$ concentration

The FTIR spectra of the olivines were obtained with the incident light along the [001] direction of olivine ( $Pbnm$  space group). The water contents that we report include the results from spectra with the electric vector parallel to the [100] and [010] directions and follow the approaches and calibrations described in Paterson (1982) and Bell et al. (2003). We did not acquire FTIR spectra with the electric vector parallel to the [001] direction and thus the water contents that we report are lower than the actual values. However, the contribution to the total water content from that direction is relatively minor in many cases (e.g., Bell et al., 2003), and is certainly <30% relative. Comparison between the water contents obtained using the Paterson (1982) and Bell et al. (2003) calibrations showed that the latter gave concentrations which are factors of 2.1–2.4 higher, similar

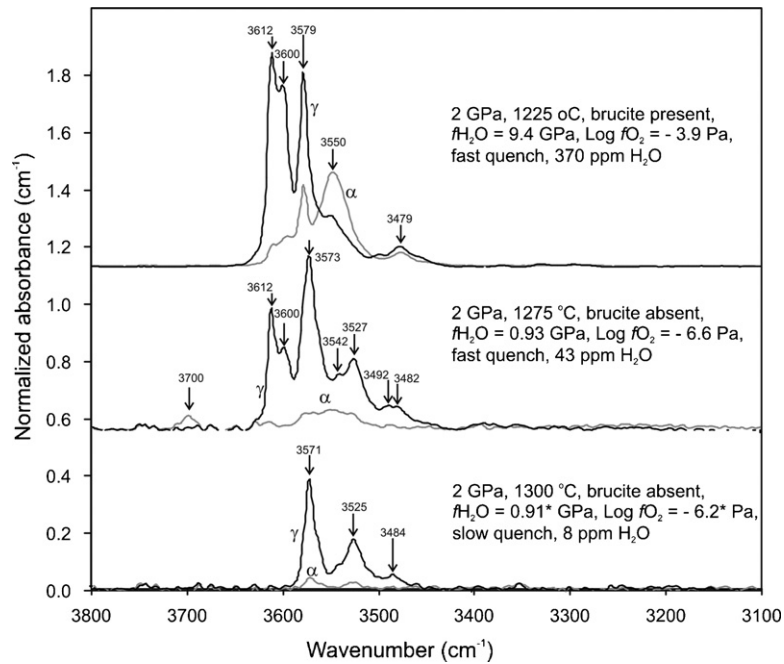


Fig. 6. FTIR spectra of three olivines annealed at different  $P$ ,  $T$ ,  $f\text{H}_2\text{O}$  and  $f\text{O}_2$  conditions. Black spectra are parallel to the  $a$  axis and gray spectra parallel to the  $b$  axis. The size of the peaks at  $3612$  and  $3600\text{ cm}^{-1}$  decrease with total water content to the extent that in the samples with the very low water (8 ppm) they are absent, a new peak appears at ca  $3527\text{ cm}^{-1}$ , and the peak at ca  $3579\text{ cm}^{-1}$  decreases and shifts to  $3571\text{ cm}^{-1}$ . The asterisk next to the  $f\text{H}_2\text{O}$  and  $f\text{O}_2$  values of the slowly cooled run is to highlight that these were calculated at the experimental conditions and are not related to the measured low water contents affected by the slow cooling and decompression path and loss of H (e.g., Fig. 5 and text for discussion).

to the value of 2.3 found by Bell et al. (2003). Using the Bell et al. (2003) calibration, the highest water content we obtain is 370 ppm  $\text{H}_2\text{O}$  from a brucite-present run at 2 GPa and  $1225\text{ }^\circ\text{C}$  that was rapidly quenched. This is  $\sim 20\%$  lower than the value of 460 ppm  $\text{H}_2\text{O}$  at water saturation obtained for the same  $P$ ,  $T$  and forsterite content with the solubility model of Zhao et al. (2004). This is an expected result because the fluid in our runs was not pure water and contained significant amounts of other C–H–O species (see below). The water content in olivines from brucite-absent runs (at 2 GPa and  $1225\text{ }^\circ\text{C}$ ) that were quenched fast is 43 ppm. The crystals from slowly quenched runs have low  $\text{H}_2\text{O}$  varying from  $\sim 7$  to 30 ppm.

FTIR spectra of olivines obtained with the electric vector parallel to the  $[100]$  direction show prominent peaks at  $3612$ ,  $3600$ ,  $3579$ ,  $3573$ ,  $3544$ ,  $3527$ , and  $3490\text{--}80\text{ cm}^{-1}$  (Fig. 6). Measurements obtained parallel to the  $[010]$  direction show much lower absorbance and less well defined peaks, some only show a bump between  $3600$  and  $3500\text{ cm}^{-1}$ , and others have peaks at  $3612$ ,  $3546$  (the most common one),  $3525$ , and  $3480\text{ cm}^{-1}$ . No significant peak was found between  $3100$  and  $3400\text{ cm}^{-1}$ . This might result from our measurements not being parallel to the  $c$  axis (e.g., Lemaire et al., 2004), although FTIR spectra of unoriented crystals annealed without brucite did not show any significant peak at these wavelengths either. There is a positive correlation between the calculated water content and the relative peak intensities for spectra parallel to the  $a$  axis. In particular, the size of the peaks at  $3612$  and  $3600\text{ cm}^{-1}$  decrease with decreasing water contents to the point where in one sample with very low water (8 ppm) they are absent. A new peak is present at ca.  $3527\text{ cm}^{-1}$ , and the peak at ca.  $3579\text{ cm}^{-1}$  decreases and shifts to  $3571\text{ cm}^{-1}$ .

A decrease in the bands at  $3612\text{ cm}^{-1}$  and  $3600\text{ cm}^{-1}$  was also observed in the experiments of Mosenfelder et al. (2006), but the bands at  $3527\text{ cm}^{-1}$  and ca.  $3579\text{ cm}^{-1}$  were absent in their study. The samples we annealed without brucite with intermediate water contents (ca. 45 ppm  $\text{H}_2\text{O}$ ) have spectra similar to that obtained from natural olivines (e.g., Miller et al., 1987).

The interpretation of the FTIR spectra and OH vibrations in terms of H in a given position of the olivine structure is a matter of intense research and interpretations (see Keppler and Bolfan-Casanova, 2006). Aside from possible effects of the relative orientation of the crystal and incident beam (e.g., Libowitzky and Rossman, 1996; Lemaire et al., 2004; our Fig. 6), the temperature, pressure (e.g., Kohlstedt et al., 1996; Zhao et al., 2004; Mosenfelder et al., 2006), oxygen fugacity (Bai and Kohlstedt, 1993), silica activity (Bai and Kohlstedt, 1993; Matveev et al., 2001; Lemaire et al., 2004), and the major and trace element composition of olivine (e.g., Zhao et al., 2004; Berry et al., 2005; Hauri et al., 2006), have been shown to influence the solubility and FTIR spectra of OH in olivine. The data we report seem to indicate spectral features may change as a function of total water content as well.

FTIR spectra of olivine has typically been interpreted considering two main possibilities: the hydrogen is associated with vacancies (Si) or point defects in the tetrahedral site in which case most peaks are at high wave numbers (e.g.,  $3650\text{--}3450\text{ cm}^{-1}$ ; Group I bands of Bai and Kohlstedt, 1993), or/and the H is associated with vacancies (e.g., Mg) or point defects (e.g.,  $\text{Fe}^{3+}$ ) in the octahedral site and the wave numbers are typically much lower ( $3450\text{--}3100\text{ cm}^{-1}$ ; group II bands of Bai and Kohlstedt, 1993). Ion microprobe measurement of H

and other trace elements in olivine annealed at water undersaturated conditions suggest a coupled substitution with H and Al replacing Si, whereas at water saturation the H incorporation mechanism changes to 2H for Mg (Hauri et al., 2006). If H is dissolved in olivine by substituting for Mg only (an issue that is not completely settled yet, e.g., see Koch-Müller et al., 2006), it needs to be clarified how Si diffusion rates are influenced by H. This is a question that we return to in the discussion section.

### 3.3. Fluid composition and calculation of water and oxygen fugacities

We obtained the ambient water and other volatile fugacities for the experimental runs in several steps. First we use the water solubility equations of Zhao et al. (2004) to obtain the  $f_{\text{H}_2\text{O}}$  from the measured OH concentration in the olivine for the quickly quenched runs only. For the brucite-absent runs the  $f_{\text{H}_2\text{O}}$  is about 0.94 GPa, and it is about 9.4 GPa when brucite was present. In a second step the fluid composition in the C–O–H system and the fugacities of  $\text{H}_2\text{O}$ ,  $\text{CO}_2$ ,  $\text{CO}$ ,  $\text{CH}_4$ ,  $\text{H}_2$ , and  $\text{O}_2$  were calculated using the  $f_{\text{H}_2\text{O}}$  obtained above and the constraint that graphite was present (i.e. activity of graphite = 1). The procedure has been described in Holloway (1987). We used a modified Redlich-Kwong equation of state (EOS) for fluids with the parameters from Holloway (1981) and considered ideal mixing. The equilibrium constants of the species forming reactions were obtained from Robie and Hemingway (1995) and the volumetric data of graphite from Holland and Powell (1998). Mixing of thermodynamic data sources was necessary because there is no single internally consistent database that contains all the data we needed. The fluid composition and fugacities that we have calculated overlap with those obtained using the Perplex thermodynamic algorithm (Connolly, 1990). Next, the ambient volatile fugacities of the slowly quenched runs were calculated using the same procedure but with the assumption that the fluid composition in these runs was the same as that obtained for the quickly quenched ones. Finally, we used the calculated  $f_{\text{H}_2\text{O}}$  and the water solubility model of Zhao et al. (2004) to obtain the concentration of OH in olivine at anneal conditions for these slowly quenched runs. The calculated water contents are 50% or more higher than the measured ones (Table 1) which is consistent with the results of the cooling and decompression diffusion model explained above (e.g., Fig. 5). The  $f_{\text{H}_2\text{O}}$  in the brucite-absent runs varies from 0.97 to 0.89 GPa (or 35–51 ppm

$\text{H}_2\text{O}$  in olivine) and  $f_{\text{O}_2}$  varies from  $10^{-7.1}$  to  $10^{-5.8}$  Pa (close to the iron–wustite oxygen fugacity buffer; Table 1) depending on temperature. For the brucite present experiments (all at 1200–1225 °C) the volatile fugacities are higher, with  $f_{\text{H}_2\text{O}} \sim 9.4$  GPa (or 370 ppm  $\text{H}_2\text{O}$  in olivine) and  $f_{\text{O}_2} \sim 10^{-3.9}$  Pa, which is close to the fayalite–magnetite–quartz oxygen fugacity buffer.

### 4. Diffusion rates of Si and O in water-bearing olivine

A finite difference algorithm was used to solve the diffusion equation and diffusion coefficients ( $D$ ) were obtained by simulating best fits to the observed isotopic profiles (Fig. 7; Table 1). We considered two media (crystal plus thin film) which were allowed to have different diffusivities; the thin film typically yielded higher values than the crystal. The position of the crystal–film interface was initially set to be the same as that of the unannealed sample that was coated and analyzed in the same batch as the sample used in the diffusion anneal. The difference between the position of the interface obtained finally from that of the unannealed sample were <100 nm and probably reflects the variability within or between thin film deposition sessions. The error of estimation of the diffusion coefficients varies, and depends on the thickness of the thin film, length of the profile, and spatial resolution of the ion microprobe session. Comparison between the results of different fits and between two different crystals from the same run shows variations of 0.1–0.2 log units and thus we have adopted errors on the diffusion coefficients of  $\pm 0.15$  log units.

A plot of  $\ln D$  vs. the inverse of temperature revealed a linear relation between the two and a least-squares routine yielded the pre-exponential factor ( $D_0$ ) and the activation energy ( $E^{\text{P}}$ ) from the relation:

$$D = D_0 \exp\left(-\frac{E^{\text{P}}}{RT}\right) \quad (1)$$

where  $R$  is the gas constant.  $E^{\text{P}}$  can be expanded into  $E^{\text{P}} = E^1 + (P - 10^5) \Delta V$ , where  $E^{\text{P}}$  is the activation energy at pressure  $P$  in Pascals,  $E^1$  is the activation energy at atmospheric pressure, and  $\Delta V$  is the activation volume. Using the data from the brucite-absent runs, we obtained: for Si,  $D_0 = 1.68 (\pm 3.52) \times 10^{-7} \text{ m}^2 \text{ s}^{-1}$  and  $E^{\text{P}} = 358 \pm 28 \text{ kJ mol}^{-1}$  (Fig. 8), and for O,  $D_0 = 1.43 (\pm 1.80) \times 10^{-4} \text{ m}^2 \text{ s}^{-1}$  and

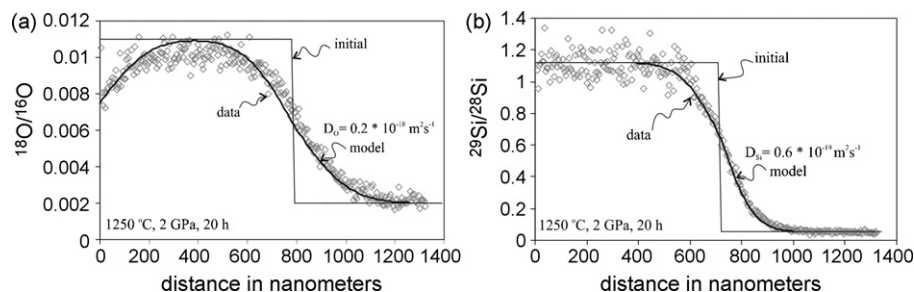


Fig. 7. Example of fits of diffusion models to the isotope concentration profiles. The initial concentration distributions were obtained in unannealed crystals. The  $\text{ZrO}_2$  layer is not detected because its O and Si isotopes have probably been homogenized by exchange with the olivine thin film. Note that the O diffusion profile (a) shows that the olivine thin film has also exchanged isotopes with the surrounding fluid.

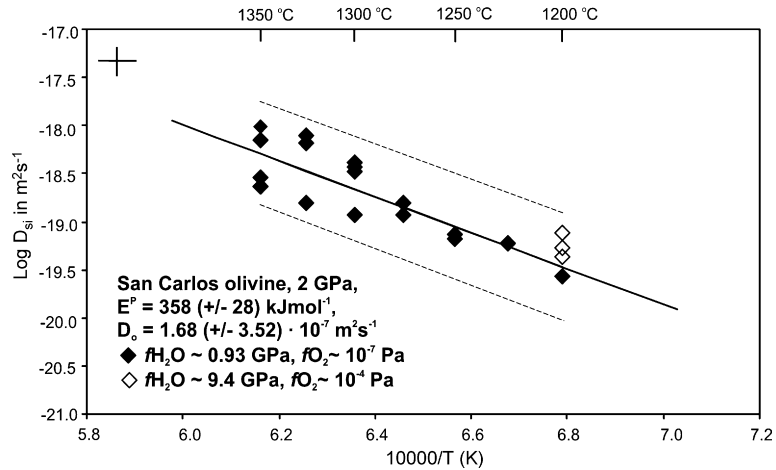


Fig. 8. Arrhenius plot for diffusion data of Si. The dashed lines are the 95% confidence intervals of the predicted values. Cross on upper left corner shows the magnitude of the error of  $D_{\text{Si}}$  and  $T$ .

$E^P = 437 \pm 17 \text{ kJ mol}^{-1}$  (Fig. 9). The Arrhenius parameters were determined by least-squares linear fits to the data and we report uncertainties at the 1 sigma level. The error on the activation energy reflect the scatter of the data which is typically larger than the estimated errors on individual measurements of  $D$  and  $T$ . A full error propagation analysis showed that incorporation of the errors on  $T$  and  $D$  quoted above changed the error on the pre exponential factor by less than 5%. Although we do not have enough Si data to define the Arrhenius parameters for the runs annealed with  $f\text{H}_2\text{O} = 9.4 \text{ GPa}$ , all data are consistent with the same activation energy (Fig. 8). Unfortunately no O diffusion data was retrieved at brucite-present runs because the diffusion profiles were too close to complete equilibration. Moreover, there is no significant difference between the diffusion coefficients measured along  $[001]$  and those obtained along  $[100]$  or  $[010]$ , implying that there is no major diffusion anisotropy in  $D_{\text{Si}}$  or  $D_{\text{O}}$  under water bearing conditions (Table 1). The O diffusion rate is about a half an order of magnitude faster than that of Si at high temperature (e.g.,  $1350^\circ\text{C}$ ) but both rates overlap at  $1150^\circ\text{C}$ . At lower temperatures, whether  $D_{\text{Si}}$  is indeed greater than  $D_{\text{O}}$  or this is an artefact of the scatter of our data remains to

be verified by direct experiments at temperatures below  $1150^\circ\text{C}$ . It is worth noting that this analysis of the data yields ‘apparent’ activation energies because it is not possible to vary  $T$ ,  $f\text{O}_2$  and  $f\text{H}_2\text{O}$  independently in high pressure experiments, and our study is no exception. A change in annealing temperature also corresponds to a change in the  $f\text{O}_2$  and  $f\text{H}_2\text{O}$  (Table 1) (see also Ganguly et al., 1998; Holzapfel et al., 2007). Thus, the  $E^P$  we have determined reflects the temperature dependence but also incorporates the effects due to variation of  $f\text{O}_2$  and  $f\text{H}_2\text{O}$  with temperature, and these need to be disentangled.

#### 4.1. Effect of variation of $f\text{H}_2\text{O}$ , $f\text{O}_2$ and $a\text{SiO}_2$ in the experiments on the retrieved values of $D_0$ and $E^P$

The variables that completely describe the system that we are dealing with (olivine plus fluid) can be determined by the Gibbs phase rule. In the water bearing case, there are five components (O, Si, Mg, Fe, H), and 5 or 6 degrees of freedom (e.g.,  $T$ ,  $P$ , Fe/Mg,  $f\text{O}_2$ ,  $a\text{SiO}_2$ , and  $f\text{H}_2\text{O}$ ) depending on whether the system is fluid saturated or not. We maintain constant  $P$ ,  $T$  and Fe/Mg in our experiments but we also need to consider  $f\text{O}_2$ ,  $f\text{H}_2\text{O}$ ,

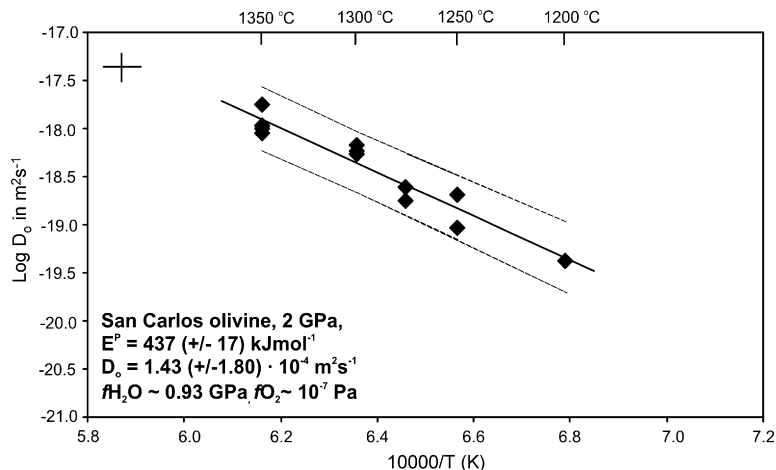


Fig. 9. Arrhenius plot for diffusion data of O. The dashed lines are the 95% confidence intervals of the predicted values. Cross on upper left corner shows the magnitude of the error of  $D_{\text{O}}$  and  $T$ .

and  $a\text{SiO}_2$ . These variables can be incorporated into the diffusion or deformation constitutive laws through exponentials (e.g., Misener, 1974), but most experimental results suggest that it is best to incorporate them in the pre-exponential factor  $D_0$  (e.g., Hirth and Kohlstedt, 2003; Dohmen and Chakraborty, 2007a). This is the form of dependence that we will consider for the subsequent analysis, i.e.:

$$D_0 = A \times f\text{O}_2^n \times f\text{H}_2\text{O}^r \times a\text{SiO}_2^m \quad (2)$$

where  $A$  is a constant,  $a\text{SiO}_2$  is the silica activity, and  $n$ ,  $r$  and  $m$  are the exponents of the independent variables.

The variation of  $f\text{H}_2\text{O}$  in the experiments used to determine  $D_0$  and  $E^{\text{P}}$  is relatively small – from 0.89 to 0.97 GPa (Table 1). If we assume for a moment that the  $f\text{H}_2\text{O}$  exponent  $r$  takes values of 1 or even 2 (e.g., Kohlstedt and Mackwell, 1998; Mei and Kohlstedt, 2000),  $D_{\text{Si}}$  or  $D_{\text{O}}$  change by a maximum factor of 1.2 over the experimental conditions of our study and thus would have a limited effect on the values of kinetic parameters that we report. This implies that the activation energies for O and Si diffusion that we derive are effectively for a constant  $f\text{H}_2\text{O}$  of ca. 0.93 ( $\pm 0.04$ ) GPa.

The effect of the  $a\text{SiO}_2$  is difficult to address since this parameter has not been directly controlled in our experiments. Dohmen et al. (2007) reported excess silica in olivine thin films deposited with the same laser conditions that we have used to produce our thin films, and thus it is likely that the activity of silica was buffered by the coexistence of silica with olivine and orthopyroxene. The same  $a\text{SiO}_2$  would be imposed by the talc of the pressure cell assembly because it breaks down to enstatite,  $\alpha$ -quartz and water vapour at the experimental  $P$ ,  $T$  conditions (e.g., Pawley and Wood, 1995; Bose and Ganguly, 1995b). Therefore, if we assume that the coexistence of enstatite and olivine defined the silica activity in our runs, then the temperature dependence of that reaction would provide us a measure of the difference in silica activity between the highest and lowest temperature runs of our study. The temperature dependence of silica activity for the enstatite-forsterite reaction is less than a factor of 1.05 for a change between 1200 °C and 1350 °C at 2 GPa (e.g., Ghiorso and Carmichael, 1987). This factor, when combined with the maximum expected exponent of  $m=4$  for many charge neutrality conditions under dry or wet conditions (e.g., Kohlstedt and Mackwell, 1998), suggests that the  $D$  values would be affected by a maximum factor of 1.2. This indicates again that the kinetic parameters for the brucite-absent runs that we report are basically derived at a constant  $a\text{SiO}_2$ . The silica activity of the brucite-present runs could have been lower than the brucite-absent and water-poor runs, with the possibility that it was controlled by the coexistence of periclase, silica and forsterite. However, whether this reaction can impose the silica activity in the diffusion zone depends on its ability to overwhelm the excess silica of the thin film (Dohmen et al., 2007).

This relatively limited variation of  $f\text{H}_2\text{O}$  and  $a\text{SiO}_2$  due to change in temperature of our experiments contrasts with a variation of about a factor of 25 in  $f\text{O}_2$  within the investigated  $T$  range ( $f\text{O}_2$  varies from  $6.3 \times 10^{-8}$  Pa to  $1.6 \times 10^{-6}$  Pa). Gérard and Jaoul (1989) and Ryerson et al. (1989) reported positive

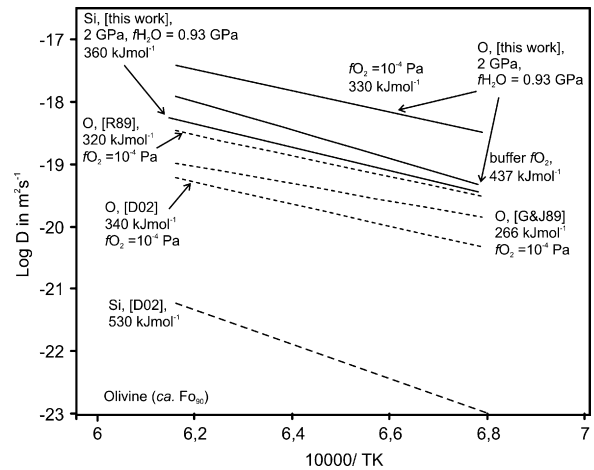


Fig. 10. Comparison of dry and water-bearing diffusion data of O and Si from various sources. [R89]: Ryerson et al. (1989); [G&J89]: Gérard and Jaoul (1989); [D02]: Dohmen et al. (2002b).

exponents that vary between 1/3 and 1/5 (determined at atmospheric pressure and dry conditions) for the dependence of  $D_{\text{O}}$  on  $f\text{O}_2$ . If we normalize the dry data of Gérard and Jaoul (1989), Ryerson et al. (1989), and Dohmen et al. (2002b) to the  $f\text{O}_2$  of our experiments, we find that (i) the activation energies obtained from the dry and wet experiments overlap (Table 2), and (ii) if the exponent  $n$  is assumed to be the same at wet and dry conditions, then the activation energy at constant  $f\text{O}_2$ , high pressures and wet conditions lies between 290 and 350  $\text{kJ mol}^{-1}$  (Fig. 10). It is interesting to note that from computer simulations it has been proposed that there is no change in the diffusion mechanism of O in pure forsterite between water bearing and dry conditions (Walker et al., 2003). For Si diffusion, Houlier et al. (1990) reported a negative dependence of the Si diffusion rate on  $f\text{O}_2$  under dry 1 atmosphere conditions and this would lead to activation energy at constant  $f\text{O}_2$ , at high pressures and wet conditions of 450  $\text{kJ mol}^{-1}$  for Si. However, the data of Houlier et al. (1990) are rather scattered and could also be fitted without any dependency on  $f\text{O}_2$ , which is in agreement with unpublished experimental results from our laboratory (R. Dohmen, personal communication). This implies that the activation energy for Si diffusion obtained by fitting the raw data remains unchanged when the effects of variation of  $a\text{SiO}_2$ ,  $f\text{H}_2\text{O}$  and  $f\text{O}_2$  with the experimental run temperatures are accounted for.

## 5. Si and O diffusion: the effect of water and pressure

The effect of water on diffusion rates can be quantified by comparing two datasets (dry and wet, or two different water fugacities) measured at constant values of the remaining variables (i.e.,  $P$ ,  $T$ ,  $\text{Fe/Mg}$ ,  $f\text{O}_2$  and  $a\text{SiO}_2$ ). This can be readily done by comparing the diffusion coefficients of Si obtained from our brucite-present and brucite-absent experiments at 1200 °C. We find that the Si diffusion rate increases on average by a factor of  $\sim 2$  for an increase of a factor of  $\sim 10$  in  $f\text{H}_2\text{O}$  (from 0.97 to 9.4 GPa). Although this average value would imply  $r=1/3$  in Eq. (2), the scatter of the data permits  $r$  to lie between 1/5 and 1 (see below).  $D_{\text{Si}}$  at  $f\text{H}_2\text{O}$  of ca. 0.93 GPa is about 2000

Table 2  
Summary of experimentally determined kinetic parameters for various elements and phenomena (diffusion and deformation) in olivine

| Material   | Crystal orientation | $D_0$ ( $\text{m}^2 \text{s}^{-1}$ ) | $E$ ( $\text{kJ mol}^{-1}$ )     | $P$ (Pa)     | $f\text{H}_2\text{O}$ (GPa) <sup>S</sup> | $f\text{O}_2$ (Pa) <sup>S</sup> | $f\text{O}_2$ exponent | $f\text{H}_2\text{O}$ exponent | $\Delta V$ ( $\times 10^{-6} \text{ m}^3 \text{ mol}^{-1}$ ) | $D$ ( $\text{m}^2 \text{ s}^{-1}$ ) or $\dot{\epsilon}$ ( $\text{s}^{-1}$ ) at 1200 °C | $\dot{D}_{\text{wet}}/\dot{D}_{\text{dry}}$ at 1200 °C, $f\text{O}_2$ corrected* | $\dot{D}_{\text{wet}}/\dot{D}_{\text{dry}}$ at 1200 °C, $f\text{O}_2$ and $P$ (2 GPa) corrected* | References and observations                                 |   |
|--|---------------------|--------------------------------------|----------------------------------|--------------|--|---------------------------------|------------------------|--------------------------------|--|--|--|--|---|---|
| Volume diffusion kinetic parameters and experimental conditions  |                     |                                      |                                  |              |  |                                 |                        |                                |  |  |  |  |   |   |
| Silicon  |                     |                                      |                                  |              |  |                                 |                        |                                |  |  |  |  |   |   |
| Water bearing  |                     |                                      |                                  |              |  |                                 |                        |                                |  |  |  |  |   |   |
| Si   | SC                  | //and $\perp$ [00 1]                 | $1.68 (\pm 3.52) \times 10^{-7}$ | $358 \pm 28$ | $2 \times 10^9$                          | 0.97                            |                        | $6.3 \times 10^{-8}$           |  | $2.7 \times 10^{-20@}$   | $2.4 \times 10^3$  | $6.0 \times 10^3$  | This study  |   |
| Si   | SC                  | //[00 1]                             |                                  |              | $2 \times 10^9$                          | 9.4                             |                        | $1.2 \times 10^{-4}$           |  | $4.3\text{--}7.5 \times 10^{-20}$  | $6.8 \times 10^3$  | $17 \times 10^3$   | This study  |   |
| Dry'   |                     |                                      |                                  |              |  |                                 |                        |                                |  |  |  |  |   |   |
| Si   | SC                  | //and $\perp$ [00 1]                 | $1.9 \times 10^{-13}$            | $291 \pm 15$ | $10^5$                                   |                                 |                        | $10^{-5}\text{--}10^{-1}$      | -1/5   | $0.7 (\pm 2.3)$  |  |  | Houlier et al. (1990), $\Delta V$ from Béjina et al. (1999) |   |
| Si   | Fo <sub>93</sub>    | //[00 1]                             | $6.3 \times 10^{-5}$             | $529 \pm 41$ | $10^5$                                   |                                 |                        | $10^{-4}$                      |  | $1.1 \times 10^{-23}$  |  |  | Dohmen et al. (2002a, b)                                    |   |
| Si pp  | Fo <sub>93</sub>    | //[00 1]                             |                                  | 540          | $2 \times 10^9$                          |                                 |                        |                                |  | $7.0 \text{€}$   |  |  | Dohmen et al. (2002a, b) normalized for $P$                 |   |
| Oxygen   |                     |                                      |                                  |              |  |                                 |                        |                                |  |  |  |  |   |   |
| Water bearing  |                     |                                      |                                  |              |  |                                 |                        |                                |  |  |  |  |   |   |
| O  | SC                  | //and $\perp$ [00 1]                 | $1.43 (\pm 1.80) \times 10^{-4}$ | $437 \pm 17$ | $2 \times 10^9$                          | 0.97                            |                        | $6.3 \times 10^{-8}$           |  | $4.6 \times 10^{-20}$  |  |  | This study  |   |
| Onn  | SC                  | //and $\perp$ [00 1]                 | $1.2 \times 10^{-6}$             | 324          | $2 \times 10^9$                          | 0.97                            |                        | $10^{-4}$                      | 1/4%   | $3.3 \times 10^{-19}$  |  |  | This study, constant $f\text{O}_2$                          |   |
| Dry'   |                     |                                      |                                  |              |  |                                 |                        |                                |  |  |  |  |   |   |
| O  | SC                  | //[100]                              | $2.6 \times 10^{-10}$            | $266 \pm 11$ | $10^5$                                   |                                 |                        | $10^{-4}$                      | 1/5  | $1.5 \times 10^{-20}$  | 22   |  | Ryerson et al. (1989)                                       |   |
| Opp  | SC                  | //[100]                              |                                  | 277          | $2 \times 10^9$                          |                                 |                        | $10^{-4}$                      |  | $7.0 \text{€}$   |  | 54   | Ryerson et al. (1989) normalized for $P$                    |   |
| O  | SC                  | //[00 1]                             | $6.7 \times 10^{-6}$             | $318 \pm 17$ | $10^5$                                   |                                 |                        | $10^{-4}$                      | 1/3  | $3.1 \times 10^{-20}$  | 11   |  | Gérard and Jaoul (1989)                                     |   |
| Opp  | SC                  | //[00 1]                             |                                  | 329          | $2 \times 10^9$                          |                                 |                        | $10^{-4}$                      |  | $7.0 \text{€}$   |  | 27   | Gérard and Jaoul (1989) corrected for $P$                   |   |
| O  | Fo <sub>93</sub>    | //[00 1]                             | $4.6 \times 10^{-9}$             | $338 \pm 14$ | $10^5$                                   |                                 |                        | $10^{-4}$                      |  | $4.7 \times 10^{-21}$  | 70   |  | Dohmen et al. (2002b)                                       |   |
| Opp  | Fo <sub>93</sub>    | //[00 1]                             |                                  | 349          | $2 \times 10^9$                          |                                 |                        | $10^{-4}$                      |  | $7.0 \text{€}$   |  | 173  | Dohmen et al. (2002b) corrected for $P$                     |   |
| Iron-magnesium   |                     |                                      |                                  |              |  |                                 |                        |                                |  |  |  |  |   |   |
| Water saturated  |                     |                                      |                                  |              |  |                                 |                        |                                |  |  |  |  |   |   |
| Fe–Mg  | Fo <sub>86</sub>    | //[00 1]                             | $10^{-14.8 (\pm 2.7)}$           | $220 \pm 60$ | $10^5$                                   | 0.97                            |                        | $10^{-2.3\text{€}}$            |  | $0.9 \pm 0.3$  | $16 (\pm 6.0)$   | $2.2 \times 10^{-16}$ (at 2 GPa)   |   | Hier-Majumder et al. (2005)   |
| Dry'   |                     |                                      |                                  |              |  |                                 |                        |                                |  |  |  |  |   |   |
| Fe–Mg  | Fo <sub>86</sub>    | //[00 1]                             | $10^{-9.2\#}$                    | $200\#$      | $10^5$                                   |                                 |                        | $10^{-2.3}$                    | 1/6 <sup>#</sup>   | 7.0  |  | $1.2 \times 10^{-16}$ (at 2 GPa)   | 2   | Dohmen and Chakraborty (2007a,b), $\Delta V$ from Holzapfel et al. (2007) |
| Dislocation creep kinetic parameters and experimental conditions |                     |                                      |                                  |              |  |                                 |                        |                                |  |  |  |  |   |   |
| Water-bearing, constant OH                                       |                     |                                      |                                  |              |  |                                 |                        |                                |  |  |  |  |   |   |
| SC grain aggregates  | SC grain aggregates |                                      |                                  | $480 \pm 40$ | $10^5$                                   | 0.97                            |                        |                                |  | 1.2  | 11   | $2.3 \times 10^{-5}$ (at 2 GPa)  | 304–1321  | Hirth and Kohlstedt (2003), $\sigma = 150$ MPa                            |
| Dry  |                     |                                      |                                  |              |  |                                 |                        |                                |  |  |  |  |   |   |
| SC grain aggregates  | SC grain aggregates |                                      |                                  | $530 \pm 40$ | $10^5$                                   |                                 |                        |                                |  |  | 13–27  | $1.7\text{--}7.4 \times 10^{-8}$ (at 2 GPa)  |   | Hirth and Kohlstedt (2003), $\sigma = 150$ MPa                            |

Notes and keys to the symbols: ( $\perp$ ) Perpendicular to an axis and ( $//$ ) parallel to an axis. The dry data for Si here refers to Dohmen et al. (2002b). ( $\text{€}$ ) These values are for  $T = 1200$  °C and 2 GPa (where applicable) and are those used in the calculation of the rate constants. (\*) Normalization not always necessary.  $\dot{\epsilon}$  is the strain rate;  $\dot{\sigma}$  is the differential stress. ( $\text{D}$ ) Diffusivity and strain rate. The labels or data followed by 'na' indicates normalization to a constant  $f\text{O}_2$ , and those followed by 'pp' normalization to 2 GPa. ( $@$ ) Measured data not calculated with the kinetic parameters. SC: San Carlos olivine (Fo<sub>92</sub>). ( $\text{€}$ ) This activation volume is taken to be the same as that for Fe–Mg (Holzapfel et al., 2007). ( $\%$ ) Value assumed intermediate between the 1/3 and 1/5 exponents determined by Gérard and Jaoul (1989) and Ryerson et al. (1989), respectively. ( $\#$ ) Values vary depending on  $f\text{O}_2$  (see Dohmen and Chakraborty, 2007a,b). ( $\text{€}$ ) This  $f\text{O}_2$  corresponds to the Ni–NiO buffer (calibration of Huebner and Sato, 1970) used by Hier-Majumder et al. (2005) at the appropriated  $P$  and  $T$ .

times, and  $D_{\text{O}}$  about 10–70 times, faster (at 1200 °C) than those at 1 atm. and dry conditions (see Table 2), if the pressure effect is ignored as a first approximation. Thus, taken on face value, these data indicate a large effect of water on Si diffusion and a smaller effect on O diffusion.

### 5.1. Analysis of the relation between water fugacity and transport properties

A diffusion coefficient ( $D^{\text{w}}$ ) in a water bearing system is given by

$$D^{\text{w}} = A^{\text{w}} f_{\text{O}_2}^{n^{\text{w}}} f_{\text{H}_2\text{O}}^r a_{\text{SiO}_2}^{\text{mw}} \exp\left(-\frac{E^{\text{1w}} + (P - 10^5)\Delta V^{\text{w}}}{RT}\right), \quad (3)$$

where the letter w in the superscripts indicates “water bearing”. For a set of data where everything other than water fugacity ( $f_{\text{H}_2\text{O}}$ ) is held constant, one obtains

$$\ln D^{\text{w}} = A' + r \ln f_{\text{H}_2\text{O}}, \quad (4)$$

with  $A' = \ln(A^{\text{w}} f_{\text{O}_2}^{n^{\text{w}}} a_{\text{SiO}_2}^{\text{mw}}) + \left(-\frac{E^{\text{1w}}}{RT}\right)$ , using  $E^{\text{Pw}} = E^{\text{1w}} + (P - 10^5)\Delta V^{\text{w}}$ . Analogously, for dry conditions, one can write:

$$D^{\text{d}} = B^{\text{d}} f_{\text{O}_2}^{n^{\text{d}}} a_{\text{SiO}_2}^{\text{md}} \exp\left(-\frac{E^{\text{1d}} + (P - 10^5)\Delta V^{\text{d}}}{RT}\right) \quad (5)$$

for diffusion in olivine of a given composition, where the superscript “d” stands for dry. This can be reduced to

$$\ln D^{\text{d}} = B' + B'' \Delta V^{\text{d}}, \quad (6)$$

with  $B' = \ln(B^{\text{d}} f_{\text{O}_2}^{n^{\text{d}}} a_{\text{SiO}_2}^{\text{md}}) + \left(-\frac{E^{\text{1d}}}{RT}\right)$ , and  $B'' = [- (P - 10^5)/RT]$ .

Eq. (3)–(6) allow the wet to dry transition to be explored in a number of ways (Fig. 11). First, wet data from two different water fugacities may be used to obtain  $r$ , as the slope of a line on a plot of  $\ln D^{\text{w}}$  vs.  $\ln f_{\text{H}_2\text{O}}$  (e.g. for Si diffusion data in this study). Secondly, values of  $r$  obtained from independent constraints (e.g. point defect models) may be used to explore the likely variation

of a diffusion coefficient with water fugacity (e.g. for O diffusion data, see below). Thirdly, Eqs. (4) and (6) may be equated to obtain the condition for transition from “dry” to “wet” behavior as a function of  $P$ ,  $T$ , etc.,

$$A' + r \ln f_{\text{H}_2\text{O}}^* = B' + B'' \Delta V^{\text{d}},$$

where  $f_{\text{H}_2\text{O}}^*$  is the value of  $f_{\text{H}_2\text{O}}$  at which the transition occurs.  $f_{\text{H}_2\text{O}}^*$  can be determined if the values of  $r$  and  $\Delta V^{\text{d}}$  are known. More usefully, the poorly constrained variables  $r$  and  $\Delta V^{\text{d}}$  can be varied within reasonable limits to obtain a plausible range for the very important parameter  $f_{\text{H}_2\text{O}}^*$  for a number of physical properties. Note that this analysis considers the wet to dry transition to occur as a kink at a point,  $f_{\text{H}_2\text{O}}^*$ , whereas in practice the transition may be smeared continuously over a range of  $f_{\text{H}_2\text{O}}$  values centered about  $f_{\text{H}_2\text{O}}^*$ . Equations similar to (3)–(6) can be written for diffusion of other species (e.g. Fe–Mg), deformation and electrical conductivity (e.g. see Hirth and Kohlstedt, 2003; Hier-Majumder et al., 2005; Karato, 2006). For dislocation creep, a related form of the equation is used (e.g. Hirth and Kohlstedt, 2003):

$$\dot{\epsilon} = A_{\text{def}} \sigma^{ne} f_{\text{H}_2\text{O}}^r \exp\left(-\frac{E^{\text{1}} + P \Delta V}{RT}\right) \quad (7)$$

Here  $\dot{\epsilon}$  = strain rate,  $A_{\text{def}}$  is a constant that includes the effects of  $f_{\text{O}_2}$  and  $a_{\text{SiO}_2}$ ,  $\sigma$  is differential stress, ‘ne’ is the differential stress exponent ( $=3.5 \pm 0.3$ ; Hirth and Kohlstedt, 2003), and the rest of the symbols have the usual meanings. As above, the various exponents and activation parameters have different values for “wet” and “dry” dislocation creep.

### 5.2. Diffusion of silicon and oxygen

The activation volume for Si diffusion under dry conditions determined between 4 and 9 GPa and at 1490 °C was found to be around zero,  $\Delta V_{\text{D}_{\text{Si}}}^{\text{d}} = 0.7 (\pm 2.3) \times 10^{-6} \text{ m}^3 \text{ mol}^{-1}$  (Béjina et al., 1999). The only other activation volume determined for diffusion in olivine at dry conditions is that of Fe–Mg, which varies between 4 and  $7 \times 10^{-6} \text{ m}^3 \text{ mol}^{-1}$  (Misener, 1974; Farber et al., 2000; Holzapfel et al., 2007), and a value for  $\Delta V_{\text{D}_{\text{Fe–Mg}}}^{\text{d}}$  of  $7 \times 10^{-6} \text{ m}^3 \text{ mol}^{-1}$  was determined for a constant  $f_{\text{O}_2}$  (see discussion in Holzapfel et al., 2007). Note that this value is significantly smaller than the wet activation volume for the diffusion of the same elements,  $\Delta V_{\text{D}_{\text{Fe–Mg}}}^{\text{w}}$  of  $16 (\pm 6) \times 10^{-6} \text{ m}^3 \text{ mol}^{-1}$  (Hier-Majumder et al., 2005). Karato (2006) suggests, based on a model of homologous temperature scaling or elastic strain energy, that the activation volume for Si diffusion in olivine should be similar to that for Mg–Fe diffusion. We will therefore consider two extreme values for  $\Delta V_{\text{D}_{\text{Si}}}^{\text{d}}$ —an activation volume of zero and one equal to that of Fe–Mg at a constant  $f_{\text{O}_2}$  (for dry conditions). A plot of  $\log f_{\text{H}_2\text{O}}$  vs.  $\log D$  of the water bearing and dry data together with lines for the exponent,  $r$ , of 2, 1, 0.5 and 0.2 is shown in Fig. 12. Combining these observations with constraints from point defect thermodynamics and charge neutrality conditions that have been considered in the literature (see below), we find that values of  $r$  between 0.5 and 1 are most likely. With the permissible limiting expo-

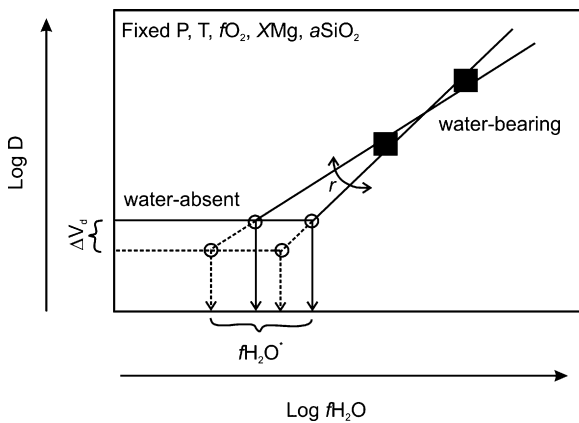


Fig. 11. Schematic diagram showing how the water fugacity exponents ( $r$  values) and the wet to dry transition ( $f_{\text{H}_2\text{O}}^*$  values) can be determined graphically. See text for more explanation.

nents of 0.2 and 1, the values of  $\log f\text{H}_2\text{O}^*$  vary between ca.  $-10$  and  $6.2$  Pa, corresponding to  $<0.1$  ppm  $\text{H}_2\text{O}$  in the olivine (Table 3) if the water solubility model of Zhao et al. (2004) is used. Varying the values of  $\Delta V_{D_{\text{Si}}}^d$  down to zero or changing  $T$  by  $\pm 100^\circ\text{C}$  to explore uncertainties does not alter the observation that the wet to dry transition occurs at  $<5$  ppm  $\text{H}_2\text{O}$  in the olivine (Table 3). These water contents are even lower than those measured in many olivine crystals from mantle xenoliths (e.g., Bell and Rossman, 1992) at the surface. The implication is that to properly model the Si diffusion rates in the mantle we need to use the water-bearing rather than dry kinetic parameters.

To analyse the effect of water on the diffusivity of oxygen, we need to consider in addition that this diffusivity depends on  $f\text{O}_2$ . We have normalized the dry diffusion data to the same  $f\text{O}_2$  as that of our experiments ( $f\text{O}_2 = 6.3 \times 10^{-8}$  Pa) using the exponent,  $n$ , of  $1/3$  (Gérard and Jaoul, 1989),  $1/5$  (Ryerson et al., 1989), or an intermediate value of  $1/4$  (Dohmen et al., 2002b). The activation volume for  $D_{\text{O}}$  under dry conditions is unknown and so we have varied  $\Delta V_{D_{\text{O}}}^d$  from zero to  $7 \times 10^{-6} \text{ m}^3 \text{ mol}^{-1}$  following the data and approach for Fe–Mg and Si noted above (Fig. 12 and Table 3). For the same ranges of water fugacity exponents ( $r=2, 1, 1/2, \text{ and } 1/5$ ) the  $\log f\text{H}_2\text{O}^*$  values for O are in general higher than those of Si, varying from about 8.2 to ca. 1 Pa. Nonetheless, they also correspond to water contents

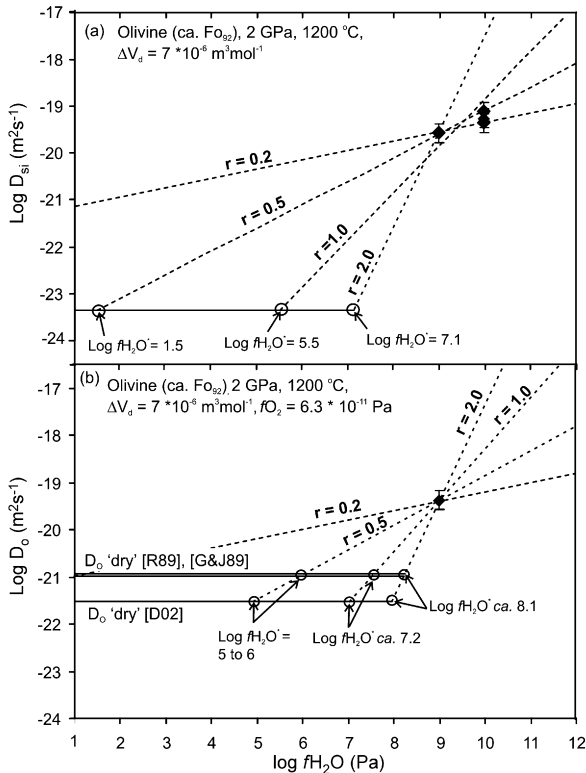


Fig. 12. Water fugacity exponents and dry to wet transitions for Si and O at  $1200^\circ\text{C}$  and  $2$  GPa. (a) The available data for Si at two  $f\text{H}_2\text{O}$  can be reproduced by water exponents between 1 and 0.2. The diffusion coefficient at dry conditions (e.g., horizontal line) is that of Dohmen et al. (2002b) using an activation volume of  $7 \text{ m}^3 \text{ mol}^{-1}$  as discussed in the text. (b) Because we have been able to retrieve the diffusion coefficient of O at a single  $f\text{H}_2\text{O}$  we cannot put strong constraint on the precise value of the  $f\text{H}_2\text{O}$  exponent for this element. Abbreviations for the references of the water absent data are as in Fig. 10.

Table 3

Log water fugacity values ( $f\text{H}_2\text{O}^*$ ) for the wet to dry transition in olivine for various transport phenomena and three representative water fugacity exponents at  $1200^\circ\text{C}$  and  $2$  GPa

| Log $f\text{H}_2\text{O}^*$ (Pa) and $\text{H}_2\text{O}$ ppm in olivine | $f\text{H}_2\text{O}$ exponent $r$ |                                  |                 |               |
|--|------------------------------------|----------------------------------|-----------------|---------------|
|  | 2                                  | 1                                | 1/2             | 1/5           |
| Si volume diffusion  | 7.1–8.1<br>0.5–5                   | 5.2–6.2<br><0.1                  | 1.5–2.5<br><0.1 | <–10<br><<0.1 |
| O volume diffusion   | 7.9–8.4<br>3–9                     | 6.9–7.8<br>0.3–2                 | 5.1–6.4<br><0.1 | <1<br><0.1    |
| Fe–Mg volume diffusion   |                                    | 8.5 <sup>a</sup><br>11           |                 |               |
| Dislocation creep  |                                    | 6.1–7.0 <sup>b</sup><br><0.1–0.4 |                 |               |

Notes and keys to the symbols: For Si and O diffusion the variation on  $\log f\text{H}_2\text{O}^*$  values correspond to varying  $\Delta V_d$  from 0 to of  $7 \times 10^{-6} \text{ m}^3 \text{ mol}^{-1}$ . For oxygen diffusion the values were calculated at the experimental conditions ( $f\text{O}_2 = 6.3 \times 10^{-8}$  Pa) and the variation also includes the difference between the dry diffusion data of Gérard and Jaoul (1989), Ryerson et al. (1989), and Dohmen et al. (2002b).

<sup>a</sup> Exponent is 0.9 (Hier-Majumder et al., 2005). The transition of dry to wet for Fe–Mg was obtained at  $\text{Fo}_{86}$ , NNO ( $f\text{O}_2 = 10^{-2.3}$  Pa) and using the equation for dry diffusion of Dohmen and Chakraborty (2007a,b).

<sup>b</sup> Exponent is 1.2, and the variation arises from using  $\Delta V_d$  of  $13\text{--}27 \times 10^{-6} \text{ m}^3 \text{ mol}^{-1}$ , using values for a constant water content using the power law parameters in Hirth and Kohlstedt (2003) with  $\sigma = 150$  MPa.

in olivine of  $<0.1\text{--}10$  ppm  $\text{H}_2\text{O}$ . Changing the  $f\text{O}_2$  dependence of O diffusivity has a limited effect on the  $\log f\text{H}_2\text{O}^*$  values (not shown). Thus, for O diffusion as well we can conclude that “wet” diffusion laws apply to most mantle olivines.

The data we have for Si diffusion suggests an  $r$  exponent between 0.5 and 1 whereas no quantitative constraint can be derived for this exponent for O. We have calculated the kinetic parameters for Si diffusion incorporating explicitly the effect of water (Eq. (2)) and using the mean value of  $f\text{H}_2\text{O}$  ( $=0.93$  GPa) from our experiments:

$$D_{\text{Si}}^w (\text{m}^2 \text{ s}^{-1}) = \alpha_{\text{Si}}^w (\text{m}^2 \text{ s}^{-1} \text{ Pa}^{-1}) f_{\text{H}_2\text{O}}^r (\text{Pa}) \times \exp\left(-\frac{358 \text{ kJ mol}^{-1} \pm 28}{RT}\right)$$

Here, if  $r=1$ ,  $\alpha_{\text{Si}}^w$  is  $1.8 \times 10^{-16}$  and if  $r=0.5$ ,  $\alpha_{\text{Si}}^w$  is  $5.5 \times 10^{-12}$ . This equation is only valid for  $\log f\text{H}_2\text{O}$  ( $f\text{H}_2\text{O}$  in Pa) values higher than about 6.

## 6. Inferences from point defects models and Si and O diffusion mechanisms

The mechanisms of Si and O diffusion in olivine can be addressed by considering the point defect chemistry of olivine (Smyth and Stocker, 1975; Stocker and Smyth, 1978; Nakamura and Schmalzried, 1983; Hobbs, 1984; Kohlstedt and Mackwell, 1998, 1999; Tsai and Dieckmann, 2002; Kohlstedt, 2006; Dohmen and Chakraborty, 2007a,b). We use the Kröger and Vink (1965) notation, e.g.  $V_{\text{Me}}''$  indicates two effective negative charges for a vacancy in the octahedral metal site, whereas  $\text{Fe}_{\text{Me}}^\bullet$

Table 4  
Dependencies of point defect concentrations on water fugacity for three charge neutrality conditions

|   | $[(\text{OH})'_{\text{O}}]$ | $[(\text{OH})'_{\text{O}} - V''_{\text{Me}}]$ | $[(2(\text{OH})'_{\text{O}} - V''_{\text{Me}})]^x$ | $[V''_{\text{O}}]$ | $[O''_{\text{I}}]$ | $[V_{\text{Si}}''']$ | $[\text{Si}_i''']$ | $[\text{H}_{\text{Si}}''']$ | $[(2\text{H})_{\text{Si}}''']$ | $[(3\text{H})_{\text{Si}}''']$ | $[(4\text{H})_{\text{Si}}''']$ |
|---|-----------------------------|---|--|--------------------|--------------------|----------------------|--------------------|-----------------------------|--------------------------------|--------------------------------|--------------------------------|
| $[(\text{OH})'_{\text{O}}] = 2[V''_{\text{Me}}]$                          | 1/3                         | 2/3   | 1  | -1/3               | 1/3                | 2/3                  | -2/3               | 1                           | 4/3                            | 5/3                            | 2                              |
| $[(\text{OH})'_{\text{O}}] = [(\text{OH})'_{\text{O}} - V''_{\text{Me}}]$ | 1/2                         | 1/2   | 1  | 0                  | 0                  | 0                    | 0                  | 1/2                         | 1                              | 3/2                            | 2                              |
| $[\text{Fe}''_{\text{Me}}] = [(\text{OH})'_{\text{O}} - V''_{\text{Me}}]$ | 3/4                         | 1/4   | 1  | 1/2                | -1/2               | -1                   | 1                  | -1/4                        | 1/2                            | 5/4                            | 2                              |

The numbers are the water fugacity exponent  $r$ .

Note:  $[\text{HSi}''']$  stands for  $[(\text{OH})_0 - V''_{\text{Si}}]'''$  and analogous abbreviations have been used for the other Si vacancy complexes. Exponents taken from Kohlstedt and Mackwell (1998, 1999), Kohlstedt (2006), and Karato (2006). Shaded ones are those that agree most with the diffusion data.

indicates an effective charge of +1 for a  $\text{Fe}^{3+}$  on the Me site. Square brackets  $[\cdot]$  denote concentration of the corresponding units.

Water derived point defects can be ‘isolated’, such as  $(\text{OH}^\bullet)_\text{O}$ , or associated with other defects such as vacancies on the Me or Si sites, or with aliovalent impurities substituting in regular sites (e.g., Kurosawa et al., 1997; Brodholt and Refson, 2000; Braithwaite et al., 2003; Karato, 2006; Kohlstedt, 2006). Based on earlier studies, it has been considered likely that the relevant ‘water defect’ is  $\{2(\text{OH}^\bullet)_\text{O} - V''_{\text{Me}}\}^x$ . The main reason for this preference (Kohlstedt, 2006) is that it leads to a water fugacity exponent of  $\sim 1$ , which is the value found in water solubility (Kohlstedt et al., 1996) and Fe–Mg diffusion (Hier-Majumder et al., 2005) experiments. Thus, the vacancy concentration in the Me site would control the amount of water incorporated in olivine (Kohlstedt, 2006). A key parameter for establishing a point defect model is the charge neutrality condition. We have compiled (Table 4) the water fugacity exponents associated with the most likely charge neutrality conditions and the different point defects in olivine. Our diffusion data allows us to eliminate a subset of these possibilities at the outset. Since the diffusion rates of Si and O both increase with  $f\text{H}_2\text{O}$ , the  $r$  exponents for both elements need to be positive and only these cases need be considered further. Irrespective of further assumptions and uncertainties, this implies that the diffusion mechanisms of the two elements (Si and O) in water bearing olivine would have to be different (Table 4).

Consideration of our experimental observation that  $r$  for Si diffusion lies between 0.2 and 1 allows the choice of point defect models and diffusion mechanisms to be narrowed further down to two options only (see Table 4): (1) charge neutrality condition  $[\text{Fe}''_{\text{Me}}] = [(\text{OH}^\bullet)_\text{O} - V''_{\text{Me}}]^x$ , implying  $r=1$  for Si with interstitial diffusion or  $r=1/2$  involving Si-vacancy associates, and  $r=1/2$  for O diffusing by a vacancy mechanism, or, (2) the charge neutrality condition  $[(\text{OH}^\bullet)_\text{O}] = 2[V''_{\text{Me}}]$ , with  $r=2/3$  for Si diffusing by a vacancy or  $r=1$  via the associated complex  $\{(\text{OH}^\bullet)_\text{O} - V''_{\text{Si}}\}'''$ , and  $r=1/3$  for oxygen diffusing by an interstitial mechanism. To unequivocally resolve which of these two options apply to diffusion processes in hydrous olivine it is necessary to obtain additional experimental data. For example, determination of the  $f\text{O}_2$  dependence of O diffusion rates in olivine under water-present conditions would help to clarify the situation (the exponent,  $n$ , would be positive or negative depending on the diffusion mechanism, see Kohlstedt and Mackwell, 1999; Karato, 2006 for further details). However, based on the available observations so far it appears that the second option involving Si-vacancy or vacancy associates,

$\{(\text{OH}^\bullet)_\text{O} - V''_{\text{Si}}\}'''$ , may be the relevant mechanism for Si diffusion. The line of reasoning is as follows: (i) computer simulations of Walker et al. (2003) indicate that water incorporation does not alter the diffusion mechanism of O in forsterite, (ii) we find that the activation energies of O diffusion in mantle olivine at dry and wet conditions are very similar. If (i) and (ii) are used to infer that the mechanism of diffusion of O is the same (Note: this does not imply that the rates are the same) under wet and dry conditions, then (iii) we can use the observed mechanism of diffusion of O under dry conditions to infer the mechanism of diffusion under wet conditions. The positive correlation between  $D_\text{O}$  and  $f\text{O}_2$  (Gérard and Jaoul, 1989; Ryerson et al., 1989) suggests that oxygen diffuses by an interstitial mechanism in dry conditions. If we accept this inference, then Si has to diffuse by a different (see above), i.e. vacancy mechanism. This leads us to prefer the second option above, involving Si-vacancy or vacancy associates,  $\{(\text{OH}^\bullet)_\text{O} - V''_{\text{Si}}\}'''$ . Note that this diffusion mechanism leads to an exponent of 1 and therefore also agrees with the observations of Kohlstedt (2006).

### 6.1. Relation between Si diffusion, concentrations of vacancies, and water content

The effect of H on Si diffusion rates via vacancies can be rationalized using the relation between mobility and diffusion coefficients (e.g., Schmalzried, 1974; pp. 53–55) which leads to  $D_\text{Si} = [V_\text{Si}] \times D_{V_\text{Si}}$ , where  $V_\text{Si}$  includes all vacancy types on the silicon site, including any of the associated complexes. This shows that faster diffusion of Si at wet conditions could result from a higher number of vacancies, from a higher diffusion rate of the vacancies, or both. The question that arises then is: how is it possible to increase the vacancy concentration and diffusion coefficient of Si by such a large factor if the inferred charge neutrality conditions indicate that H mainly goes into the Me sites? To address this question, we make the assumption that diffusivities of vacancies in the olivine structure, whether they are on the metal or the tetrahedral site, are of the same order of magnitude, i.e.  $D_{V_\text{Si}} \approx D_{V_\text{Me}}$ . This is consistent with inferences already made from various physical property measurements (e.g., Mackwell et al., 1988; Wanamaker, 1994; Kohlstedt, 2006). Then it follows that  $D_\text{Si} = [V_\text{Si}] \times D_{V_\text{Si}} \approx [V_\text{Si}] D_{V_\text{Me}} = [V_\text{Si}] \times (D_{\text{Fe-Mg}}/[V_\text{Me}])$ , or,  $[V_\text{Si}] = D_\text{Si} \times ([V_\text{Me}]/D_{\text{Fe-Mg}})$ . Using this relationship, we obtain  $[V_\text{Si}^\text{d}] \approx 3 \times 10^{-12}$  using  $D_{\text{Fe-Mg}}$  from Dohmen and Chakraborty (2007a,b),  $D_\text{Si}^\text{d}$  from Dohmen et al. (2002b), and  $[V_\text{Me}^\text{d}] \approx 9 \times 10^{-5}$  from Dohmen and Chakraborty (2007a,b) (Table 5). Likewise, we obtain  $[V_\text{Si}^\text{w}] \approx 6 \times 10^{-8}$  using  $D_{\text{Fe-Mg}}$

Table 5

Diffusion coefficients ( $\text{m}^2 \text{s}^{-1}$ ) and calculated point defect concentrations at  $1200^\circ\text{C}$ ,  $2 \text{ GPa}$ ,  $f\text{O}_2 = 10^{-2.3} \text{ Pa}$

|                    | Dry                   | $f\text{H}_2\text{O} = 0.97 \text{ GPa}$ |
|--------------------|-----------------------|--|
| $D_{\text{Fe-Mg}}$ | $1.2 \times 10^{-16}$ | $2.2 \times 10^{-16}$                    |
| $D_{\text{Si}}$    | $4.5 \times 10^{-24}$ | $2.7 \times 10^{-20}$                    |
| $[V_{\text{Me}}]$  | $8.8 \times 10^{-5}$  | $4.4 \times 10^{-4}$                     |
| $[V_{\text{Si}}]$  | $3.5 \times 10^{-12}$ | $5.3 \times 10^{-8}$                     |

from Hier-Majumder et al. (2005),  $D_{\text{Si}}^{\text{w}}$  from this study, and  $[V_{\text{Me}}^{\text{w}}] \approx 4 \times 10^{-4}$  using the approach of Wang et al. (2004). The interesting aspects are that (i) the vacancy concentrations are several orders of magnitude smaller than the concentration of water dissolved in olivine, and (ii) the number of water related defects in the Me-site, e.g.,  $[V_{\text{Me}}^{\text{w}}] \approx 4 \times 10^{-4}$  whereas  $[V_{\text{Si}}^{\text{w}}] \approx 5 \times 10^{-8}$ . This means that only about 0.01% of the H that enters the olivine structure might already substantially enhance the Si vacancy concentrations (e.g. from  $[V_{\text{Si}}^{\text{d}}] \approx 3 \times 10^{-12}$  to  $[V_{\text{Si}}^{\text{w}}] \approx 5 \times 10^{-8}$ ) and therefore, the Si diffusion and dislocation creep (depending on the precise role of oxygen not considered here) rates. This analysis is also consistent with the observation that the wet to dry transition for Si diffusion occurs at much lower water contents than for Fe–Mg diffusion (see below).

## 7. The wet to dry transition for Fe–Mg diffusion and dislocation creep in olivine and their relation to Si and O diffusion

We now consider the experimental data on ionic diffusion and deformation under wet and dry conditions to try to develop an integrated understanding of how water enters the olivine structure and affects these processes. The nature of influence of water on these processes is embodied in the exponent  $r$ , the critical  $f\text{H}_2\text{O}^*$  of transition from "wet" to "dry" laws (see Section 5.1) and in the activation energies and volumes. Similarity of these values for different processes should point to similar underlying atomistic mechanisms (e.g., Karato, 2006; Kohlstedt, 2006)

### 7.1. Fe–Mg diffusion

We find that the "wet" to "dry" transition for this process occurs at  $\log f\text{H}_2\text{O}^* = 8.5$  (or about 11 ppm  $\text{H}_2\text{O}$  in the olivine) when Fe–Mg diffusion coefficients at  $2 \text{ GPa}$ ,  $1200^\circ\text{C}$ ,  $f\text{O}_2 = 10^{-2.3} \text{ Pa}$  (Ni–NiO buffer) and an olivine composition of  $\text{Fo}_{86}$  are compared (Fig. 13, wet data: Hier-Majumder et al., 2005; dry data: Dohmen and Chakraborty, 2007a,b). This transition point ( $\log f\text{H}_2\text{O}^*$ ) is about 3 log units higher than that for Si diffusion for almost the same exponent ( $r = 1$ ) (Table 3) and represents the minimum water fugacity at which the "wet" equation for Fe–Mg diffusion can be used. The enhancement of Fe–Mg diffusion rates from "dry" conditions to a  $f\text{H}_2\text{O} = 0.97 \text{ GPa}$  is only by a factor of two, compared to factors of 1000 and 50 for Si and O diffusion, respectively. Note that this enhancement of Fe–Mg diffusion is smaller than that reported by Hier-Majumder et al. (2005) because they did not normalize the dry diffusion coefficients to the oxygen fugacity of their experiments for com-

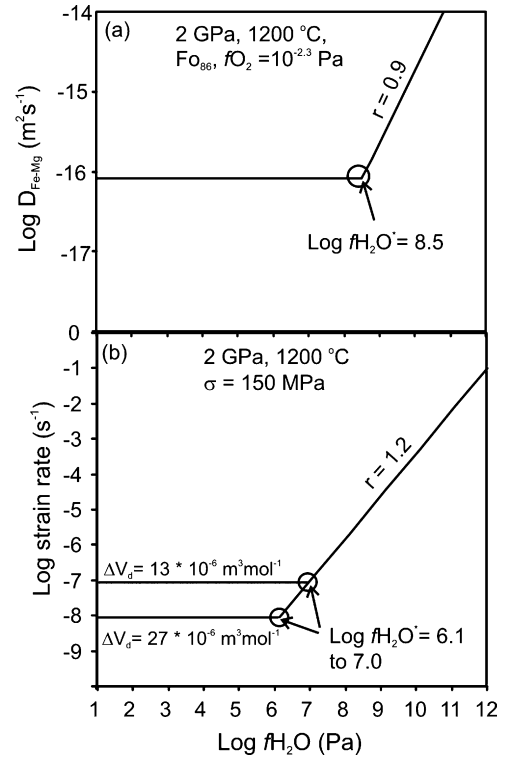


Fig. 13. Water fugacity exponents and dry to wet transitions for different transport properties in forsterite-rich single crystal olivine or aggregates. (a) Fe–Mg diffusion. Dry diffusion parameters from Dohmen and Chakraborty (2007a,b) and Holzapfel et al. (2007). Water-bearing parameters from Hier-Majumder et al. (2005). (b) Dislocation creep parameters from the review of Hirth and Kohlstedt (2003).

parison. The observations that (i) the wet to dry transition for Fe–Mg diffusion occurs at higher water fugacities than for Si and O diffusion and (ii) the effect of water on this diffusion rate is smaller than its effect on Si and O diffusion are consistent with the point defect systematics we have discussed above (Section 6.1).

### 7.2. Dislocation creep

We have carried out a similar comparison of dry and wet creep data for olivine using the constitutive laws and parameters reported by Hirth and Kohlstedt (2003), considering the uncertainties in activation volume (between  $13$  and  $27 \times 10^{-6} \text{ m}^3 \text{ mol}^{-1}$ ) and an exponent,  $r$  of  $1.2$  (Hirth and Kohlstedt, 2003; Fig. 13, Table 3). The transition point,  $\log f\text{H}_2\text{O}^*$ , lies between  $6.1$  and  $7.0$  (or,  $<0.3$  ppm water in olivine), which is similar to the value of  $\sim 7.6$  found by Mei and Kohlstedt (2000) using slightly different data. This value is two orders of magnitude below the transition point for Fe–Mg diffusion (Section 7.1) but is at the upper end of the range of values found for Si diffusion (Table 3), with the same value for the exponent,  $r$ , of  $1$ . This points to a strong connection between the process of creep and diffusion of Si in olivine (Fig. 13).

The connection can be evaluated further by considering the activation energies of different processes. Dohmen et al. (2002b) and Kohlstedt (2006) argued that diffusion of Si controls

the creep of olivine under dry conditions because the activation energies of the two processes are identical and Si is the slowest diffusing species in olivine at those conditions. In the presence of H<sub>2</sub>O, the rates of Si and O diffusion are more similar to each other and therefore it is reasonable to expect that creep may be controlled by both processes. The activation energies for the concerned processes in the presence of water are:  $358 \pm 28 \text{ kJ mol}^{-1}$  for Si diffusion,  $437 \pm 17 \text{ kJ mol}^{-1}$  for O diffusion (this study) and  $500 \pm 40 \text{ kJ mol}^{-1}$  (Hirth and Kohlstedt, 2003) or  $410 \pm 40 \text{ kJ mol}^{-1}$  (Karato, 2006) for creep. The activation energy for Si diffusion is lower than that for creep, although there is a slight overlap with the value found by Karato (2006) when errors are considered. On the other hand, the activation energy for O diffusion is very similar to the value for creep found by Karato (2006) and overlaps within error with the value obtained by Hirth and Kohlstedt (2003). Therefore, in water bearing olivine where diffusion rates of Si and O are similar, creep rate appears to be controlled by an interplay of Si and O diffusion. The exponent,  $r$ , for creep is close to that for Si diffusion and the activation energy is closer to that for O diffusion.

In summary, we find that the wet to dry transition for various physical properties (Fe–Mg diffusion, Si diffusion, O diffusion and creep) occurs at relatively low water fugacities and water contents in olivine (<10 ppm), even when all likely variation and uncertainties in various parameters are considered (Table 3). Such water concentrations are lower or similar to those measured in many mantle xenoliths or olivine xenocrysts (e.g. Bell and Rossman, 1992; Ingrin and Skogby, 2000). Thus, it can be expected that the physical properties of the upper mantle (viscosity, electrical conductivity, diffusion rates) will be affected by water even if the mantle is largely water undersaturated. This implies that experimental studies that investigate the effects of small amounts H on the physical and chemical properties of mantle materials are directly relevant to understanding the rheological and chemical evolution of mantle; the effect of H should be incorporated in numerical models of mantle dynamics (see Section 8). This finding is in agreement with studies that model the mantle flow under the western USA—these seem to require a ‘wet’ rheological law (Dixon et al., 2004; Freed and Bürgmann, 2004).

## 8. Calculating strain rates of water-bearing olivine from Si and O diffusion data

The foregoing discussions suggest a close connection between the diffusion of Si and O and dislocation creep of olivine. To quantitatively test this relation we have used our diffusion data in three creep models (following Kohlstedt, 2006) to try to reproduce the experimentally measured strain rates. In the model of Weertman (1999), most of the strain is produced by glide and only a small fraction is produced by climb, but it is dislocation climb that controls the strain rate which is given by

$$\dot{\epsilon} = 2\pi \frac{GV_m}{RT} \left(\frac{\sigma}{G}\right)^3 \frac{D_{\text{self}}}{b^2} \frac{1}{\ln(G/\sigma)} \frac{\lambda_g}{\lambda_c}$$

where  $G$  is the shear modulus,  $V_m$  is the molar volume,  $b$  is the Burgers vector,  $\lambda_g$  is the glide distance,  $\lambda_c$  is the climb distance

and  $D_{\text{self}}$  is the self-diffusivity. In the model of Nabarro (1967), with the correction of a  $2\pi$  factor due to Nix et al. (1971), all the strain is accomplished by climb and one obtains:

$$\dot{\epsilon} = 2 \frac{GV_m}{RT} \left(\frac{\sigma}{G}\right)^3 \frac{D_{\text{self}}}{b^2} \frac{1}{\ln(4G/\pi\sigma)}$$

Finally, the model of Evans and Knowles (1978) also contains the Poisson’s ratio ( $\nu$ ), and all the strain is generated by glide but the creep rate is governed by climb, given by

$$\dot{\epsilon} = \frac{4.2\sqrt{3}\pi}{\alpha^2} \frac{GV_m}{RT} \left(\frac{\sigma}{G}\right)^3 \frac{D_{\text{self}}}{b^2} \frac{1}{\ln(\alpha G/2\sigma)} \times \left\{ 1 + \frac{2}{\alpha} \left[ 1 + \frac{1}{2\pi(1-\nu)} \right] \right\}$$

where  $\alpha = 1.6$ . All three equations contain the self-diffusion coefficient, which provides a direct link between the strain rate and volume diffusion. Although  $D_{\text{self}}$  has a unique meaning in the context of the original experimental data on pure metals that were used to obtain such relations, in the case of olivine its meaning is more ambiguous. It probably relates to the flux of the entire molecule of olivine and thus requires a multicomponent ( $\tilde{D}$ ) formulation (Ruoff, 1965; Dimos et al., 1988; Jaoul, 1990; Kohlstedt, 2006). Since  $\tilde{D}$  is similar to the diffusivity of the slowest ion, we have used the values of  $D_{\text{Si}}$  or  $D_{\text{O}}$  (depending on which is the slowest) as a proxy for  $D_{\text{self}}$  to calculate the strain rates.

It is apparent that the strain rates calculated with the Nabarro (1967) model are about one order of magnitude lower than those obtained using Evans and Knowles (1978) equation and overlap with those from Weertman (1999) when  $\lambda_g/\lambda_c = 0.1$  (Fig. 14).

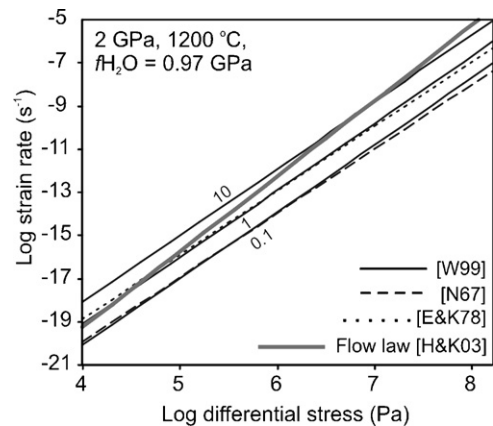


Fig. 14. Strain rates calculated using three different dislocation creep models that involve the role of climb as rate limiting step. [W99] is the model of Weertman (1999), [N67] refers to the model of Nabarro (1967) and [E&K78] refers to that of Evans and Knowles (1978). The flow law was calculated using the constant fugacity values and parameters found in Hirth and Kohlstedt (2003). The numbers next to the Weertman models are different values of  $\lambda_g/\lambda_c$ . The diffusion coefficient that was used in the dislocation creep models is  $2.7 \times 10^{-20} \text{ m}^2 \text{ s}^{-1}$  and corresponds to  $D_{\text{Si}}$  at 1200 °C, 2 GPa and  $f\text{H}_2\text{O} = 0.97 \text{ GPa}$  (Table 1). Other values used are as in Kohlstedt (2006) with  $G = 52 \text{ GPa}$ ,  $b = 0.485 \text{ nm}$ ,  $V_m = 43.8 \times 10^{-6} \text{ m}^3$ ,  $\nu = 0.245$ . Note good agreement between the flow law and the Evans and Knowles (1978) at low differential stress and with that of Weertman (1999) for  $\lambda_g/\lambda_c$  values between 1 and 10 indicating that the role of climb is important in determining the dislocation creep rates.

More significantly, the strain rates calculated using Nabarro (1967) formulation are about one to two orders of magnitude smaller than those obtained from the flow law using the values of Hirth and Kohlstedt (2003). The strain rates obtained using the expression from Evans and Knowles (1978) agree with the flow law at low differential stress ( $10^4$ – $10^5$  Pa) but underestimate them by about one order of magnitude at higher values of differential stress ( $10^7$ – $10^8$  Pa). The strain rates obtained using the equation from Weertman (1999) overlap with the flow law values if  $\lambda_g/\lambda_c$  takes values between 1 and 10. We feel that the extent of agreement between the strain rates calculated from diffusion data and those obtained from experimentally determined flow laws is rather good, in particular for low strain rates ( $<10^5$  Pa) and for models where dislocation climb has an important role in limiting creep rates, although glide causes much of the strain. The best fits are obtained if it is assumed that climb and glide of dislocations contribute about equally to dislocation creep of olivine under hydrous conditions. We would like to note here that the discrepancy in slope between strain rates calculated from diffusion data and those obtained from fits of flow laws to experimental data arise because the differential stress exponent for the models are close to 3 whereas that for the experimental fit to flow laws is higher (about 3.5, Hirth and Kohlstedt, 2003) i.e. it is intrinsic to the nature of the models.

## 9. Conclusions

Our experimental results show that even low amounts of H ( $\sim 45$  ppm  $H_2O$  in olivine) at high pressure (2 GPa) considerably enhance the diffusion rates of Si (by three orders of magnitude) and O (about one order of magnitude) compared to rates measured in water-absent mantle olivine (Dohmen et al., 2002b). Unlike the findings in dry conditions, diffusion rates of Si and O are similar under water bearing conditions and diffusion anisotropy is weak to absent. The high impact of H on Si diffusion can be understood by recognizing that the concentration of Si vacancies is about 4 orders of magnitude smaller than the amount of H that can be incorporated in olivine at the same conditions. Therefore, even a small fraction of the total incorporated H is capable of substantially increasing the concentration of defects responsible for diffusion of Si. The relation between the water fugacity and the Si diffusion rates seems to obey a power law with a water fugacity exponent of 0.2–1; the latter exponent is the same as that derived for dislocation creep of olivine. This indicates a strong connection between Si diffusion and deformation. However, the activation energy for dislocation creep is significantly higher (by ca.  $100$ – $150$  kJ mol $^{-1}$ ) than that for diffusion of Si, whereas it is within error the same as that for O diffusion. This is consistent with the observation that Si and O diffusion rates are similar under “wet” conditions, so that the two processes control different aspects of dislocation creep. For all the transport properties considered (volume diffusion and dislocation creep) the change in behavior from “dry” to “water bearing” conditions occurs at low H concentration (e.g.,  $<10$  ppm of  $H_2O$  in olivine at 2 GPa and 1200 °C). These values are lower than or overlap with those obtained from many olivine crystals from mantle xenoliths. The implication is that even if

the mantle is far from water saturated, the influence of water on kinetic data needs to be considered for understanding the physical and chemical behavior and evolution of the upper mantle—a petrologically dry mantle may be rheologically and kinetically wet.

## Acknowledgements

Many people contributed toward completion of this project. We thank R. Dohmen for many discussions on point defects and diffusion and help with the thin film deposition technique, M. Burchard for training during the piston cylinder experiments, T. Westphal for extreme care during polishing the crystal surfaces, H. Schulze in Bayreuth for drilling the crystals, H. Keppler in Bayreuth for help during FTIR analyses of olivine, J. Craven in Edinburgh for careful SIMS analyses, and H.-W. Becker for help with the Rutherford Backscattering spectroscopy. Thorough reviews by D. Kohlstedt and an anonymous reviewer helped to improve the clarity of the paper. Generous funding by the DFG under SFB project 526 made this study possible.

## References

- Bai, Q., Kohlstedt, D.L., 1992. Substantial hydrogen solubility in olivine and implications for water storage in the mantle. *Nature* 357, 672–674.
- Bai, Q., Kohlstedt, D.L., 1993. Effects of chemical environment on the solubility and incorporation mechanism for hydrogen in olivine. *Phys. Chem. Min.* 19, 460–471.
- Béjina, F., Jaoul, O., Liebermann, R.C., 1999. Activation volume of Si diffusion in San Carlos olivine: implications for upper mantle rheology. *J. Geophys. Res.* 104, 25529–25542.
- Bell, D.R., Rossman, G.R., 1992. Water in earths mantle—the role of nominally anhydrous minerals. *Science* 255, 1391–1397.
- Bell, D.R., Rossman, G.R., Maldener, J., Endisch, D., Rauch, F., 2003. Hydroxide in olivine: a quantitative determination of the absolute amount and calibration of the IR spectrum. *J. Geophys. Res.* 108, doi:10.1029/2001JB000679.
- Beran, A., Libowitzky, E., 2006. Water in natural mantle minerals. II. Olivine, garnet and accessory minerals. In: Keppler, H., Smyth, J.R. (Eds.), *Water in Nominally Anhydrous Minerals*. *Rev. Min. Geochem.* 62, 169–191.
- Beran, A., Putnis, A., 1983. A model of the oh positions in olivine derived from infrared-spectroscopic investigations. *Phys. Chem. Min.* 9, 57–60.
- Bercovici, D., Karato, S., 2003. Whole-mantle convection and the transition-zone water filter. *Nature* 425, 39–44.
- Berry, A.J., Hermann, J., O’Neill, H.S.C., Foran, G.J., 2005. Fingerprinting the water site in mantle olivine. *Geology* 33, 869–872.
- Billen, M.L., Gurnis, M., 2001. A low viscosity wedge in subduction zones. *Earth Planet. Sci. Lett.* 193, 227–236.
- Bolfan-Casanova, N., 2005. Water in the Earth’s mantle. *Min. Mag.* 69, 229–257.
- Bose, K., Ganguly, J., 1995a. Quartz–coesite transition revisited—reversed experimental-determination at 500–1200 °C and retrieved thermochemical properties. *Am. Min.* 80, 231–238.
- Bose, K., Ganguly, J., 1995b. Experimental and theoretical studies of the stabilities of talc, antigorite and phase A at high pressures with applications to subduction processes. *Earth Planet. Sci. Lett.* 136, 109–121.
- Braithwaite, J.S., Wright, K., Catlow, C.R.A., 2003. A theoretical study of the energetics and IR frequencies of hydroxyl defects in forsterite. *J. Geophys. Res.* 108, doi:10.1029/2002JB002126.
- Brodholt, J.P., Refson, K., 2000. An ab initio study of hydrogen in forsterite and a possible mechanism for hydrolytic weakening. *J. Geophys. Res.* 105, 18977–18982.
- Chakraborty, S., Ganguly, J., 1992. Cation diffusion in aluminosilicate garnets—experimental-determination in spessartine–almandine diffusion

- couples, evaluation of effective binary diffusion-coefficients, and applications. *Contrib. Min. Petrol.* 111, 74–86.
- Chakraborty, S., Rubie, D.C., 1996. Mg tracer diffusion in aluminosilicate garnets at 750–850 °C, 1 atm. and 1300 °C, 8.5 GPa. *Contrib. Min. Petrol.* 122, 406–414.
- Connolly, J.A.D., 1990. Multivariable phase-diagrams—an algorithm based on generalized thermodynamics. *Am. J. Sci.* 290, 666–718.
- Demouchy, S., Mackwell, S., 2003. Water diffusion in synthetic iron-free forsterite. *Phys. Chem. Min.* 30, 486–494.
- Demouchy, S., Mackwell, S., 2006. Mechanisms of hydrogen incorporation and diffusion in iron-bearing olivine. *Phys. Chem. Min.* 33, 347–355.
- Demouchy, S., Mackwell, S.J., Kohlstedt, D.L., 2007. Influence of hydrogen on Fe–Mg interdiffusion in (Mg, Fe)O and implications for Earth’s lower mantle. *Contrib. Min. Petrol.* 154 (3), 279–289.
- Dimos, D., Wolfenstine, Kohlstedt, D.L., 1988. Kinetic demixing and decomposition of multicomponent oxides due to a nonhydrostatic stress. *Acta Metall.* 36, 1543–1552.
- Dixon, J.E., Dixon, T.H., Bell, D.R., Malservisi, R., 2004. Lateral variation in upper mantle viscosity: role of water. *Earth Planet. Sci. Lett.* 222, 451–467.
- Dohmen, R., Chakraborty, S., 2007a. Fe–Mg diffusion in olivine II: point defect chemistry, change of diffusion mechanisms and a model for calculation of diffusion coefficients in natural olivine. *Phys. Chem. Min.* 34 (6), 409–430.
- Dohmen, R., Chakraborty, S., 2007b. Fe–Mg diffusion in olivine II: point defect chemistry, change of diffusion mechanisms and a model for calculation of diffusion coefficients in natural olivine (vol. 34, 2007, p. 409). *Phys. Chem. Min.* 34 (8), 597–598.
- Dohmen, R., Chakraborty, S., Becker, H.W., 2002b. Si and O diffusion in olivine and implications for characterizing plastic flow in the mantle. *Geophys. Res. Lett.* 29, doi:10.1029/2002GL015480.
- Dohmen, R., Becker, H.-W., Chakraborty, S., 2007. Fe–Mg diffusion in olivine. I. Experiments determination between 700 and 1200 °C as a function of composition, crystal orientation and oxygen fugacity. *Phys. Chem. Min.* 34 (6), 389–407.
- Dohmen, R., Becker, H.W., Meissner, E., Etzel, T., Chakraborty, S., 2002a. Production of silicate thin films using pulsed laser deposition (PLD) and applications to studies in mineral kinetics. *Eur. J. Min.* 14, 1155–1168.
- Elphick, S.C., Ganguly, J., Loomis, T.P., 1985. Experimental-determination of cation diffusivities in aluminosilicate garnets. I. Experimental methods and interdiffusion data. *Contrib. Min. Petrol.* 90, 36–44.
- Evans, H.E., Knowles, G., 1978. Dislocation creep in non-metallic materials. *Acta Metall.* 26, 141–145.
- Farber, D.L., Williams, Q., Ryerson, F.J., 2000. Divalent cation diffusion in Mg<sub>2</sub>SiO<sub>4</sub> spinel (ringwoodite), beta phase (wadsleyite), and olivine: implications for the electrical conductivity of the mantle. *J. Geophys. Res.* 105, 513–529.
- Freed, A.M., Bürgmann, R., 2004. Evidence of power-law flow in the Mojave desert mantle. *Nature* 430, 548–551.
- Ganguly, J., Bhattacharya, R.N., Chakraborty, S., 1988. Convolution effect in the determination of compositional profiles and diffusion-coefficients by microprobe step scans. *Am. Min.* 73, 901–909.
- Ganguly, J., Cheng, W.J., Chakraborty, S., 1998. Cation diffusion in aluminosilicate garnets: experimental determination in pyrope-almandine diffusion couples. *Contrib. Min. Petrol.* 131, 171–180.
- Gérard, O., Jaoul, O., 1989. Oxygen diffusion in San-Carlos Olivine. *J. Geophys. Res.* 94, 4119–4128.
- Ghiorso, M.S., Carmichael, I.S.E., 1987. Modeling magmatic systems—petrologic applications. In: Carmichael, I.S.E., Eugster, H.P. (Eds.), *Thermodynamic Modelling of Geological Materials: Minerals, Fluids and Melts*. *Rev. Min.* 17, 467–499.
- Goldsmith, J.R., 1991. Pressure enhanced Al/Si diffusion and oxygen isotope exchange. In: Ganguly, J. (Ed.), *Diffusion, Atomic Ordering, and Mass Transport*. *Adv. Phys. Chem.* 8, 221–247.
- Graham, C.M., Elphick, S.C., 1991. Some experimental constraints on the role of hydrogen in oxygen and hydrogen diffusion and Al–Si interdiffusion in silicates. In: Ganguly, J. (Ed.), *Diffusion, Atomic Ordering, and Mass Transport*. *Adv. Phys. Chem.* 8, 248–303.
- Hauri, E.H., Gaetani, G.A., Green, T.H., 2006. Partitioning of water during melting of the Earth’s upper mantle at H<sub>2</sub>O-undersaturated conditions. *Earth Planet. Sci. Lett.* 248, 715–734.
- Hier-Majumder, S., Anderson, I.M., Kohlstedt, D.L., 2005. Influence of protons on Fe–Mg interdiffusion in olivine. *J. Geophys. Res.* 110, doi:10.1029/2004JB003292.
- Hirschmann, M.M., 2006. Water, melting, and the deep Earth H<sub>2</sub>O cycle. *Annu. Rev. Earth Planet. Sci.* 34, 629–653.
- Hirth, G., Kohlstedt, D.L., 1996. Water in the oceanic upper mantle: Implications for rheology, melt extraction and the evolution of the lithosphere. *Earth Planet. Sci. Lett.* 144, 93–108.
- Hirth, G., Kohlstedt, D., 2003. Rheology of the upper mantle and the mantle wedge: a view from the experimentalist. In: Eiler, J. (Ed.), *Inside the Subduction Factory*. *Am. Geophys. Union, Monogr.* 138, 83–105.
- Hobbs, B.E., 1984. Point-defect chemistry of minerals under a hydrothermal environment. *J. Geophys. Res.* 89, 4026–4038.
- Holland, T.J.B., Powell, R., 1998. An internally consistent thermodynamic data set for phases of petrological interest. *J. Metam. Geol.* 16, 309–343.
- Holloway, J.R., 1981. Compositions and volumes of supercritical fluids in the Earth’s crust. In: Hollister, L.S., Crawford, M.L. (Eds.), *Fluid Inclusions, Applications to Petrology*, pp. 13–38 (Mineralogical Association of Canada).
- Holloway, J.R., 1987. Igneous fluids. In: Carmichael, I.S.E., Eugster, H.P. (Eds.), *Thermodynamic Modelling of Geological Materials: Minerals, Fluids and Melts*. *Rev. Min.* 17, 211–233.
- Holzappel, C., Chakraborty, S., Rubie, D.C., Frost, D.J., 2007. Effect of pressure on Fe–Mg, Ni and Mn diffusion in (Fe<sub>x</sub>Mg<sub>1-x</sub>)SiO<sub>4</sub>. *Phys. Earth Planet. Int.*, in press.
- Houlier, B., Cheraghmakani, M., Jaoul, O., 1990. Silicon diffusion in San-Carlos Olivine. *Phys. Earth Planet. Int.* 62, 329–340.
- Huebner, J.S., Sato, M., 1970. Oxygen fugacity–temperature relationships of manganese oxide and nickel oxide buffers. *Am. Min.* 55, 934–952.
- Ingrin, J., Skogby, H., 2000. Hydrogen in nominally anhydrous upper-mantle minerals: concentration levels and implications. *Eur. J. Min.* 12, 543–570.
- Jaoul, O., 1990. Multicomponent diffusion and creep in olivine. *J. Geophys. Res.* 95, 17631–17642.
- Johnson, M.C., Walker, D., 1993. Brucite [Mg(OH)<sub>2</sub>] dehydration and the molar volume of H<sub>2</sub>O to 15 GPa. *Am. Min.* 78, 271–284.
- Karato, S., 2006. Influence of hydrogen-related defects on the electrical conductivity and plastic deformation of mantle minerals: a critical review. In: Jacobsen, S.D., van der Lee, S. (Eds.), *Earth’s Deep Water Cycle*. *Geophys. Monog. Ser.* 168, 113–130.
- Karato, S.I., Jung, H., 2003. Effects of pressure on high-temperature dislocation creep in olivine. *Phil. Mag.* 83, 401–414.
- Keppler, H., Bolfan-Casanova, N., 2006. Thermodynamics of water solubility and partitioning. In: Keppler, H., Smyth, J.R. (Eds.), *Water in Nominally Anhydrous Minerals*. *Rev. Min. Geochem.* 62, 193–230.
- Koch-Müller, M., Matsyuk, S.S., Rhede, D., Wirth, R., Khisina, N., 2006. Hydroxyl in mantle olivine xenocrysts from the Udachnaya kimberlite pipe. *Phys. Chem. Min.* 33, 276–287.
- Kohlstedt, D.L., 2006. The role of water in high-temperature rock deformation. In: Keppler, H., Smyth, J.R. (Eds.), *Water in Nominally Anhydrous Minerals*. *Rev. Min. Geochem.* 62, 377–396.
- Kohlstedt, D.L., Mackwell, S.J., 1998. Diffusion of hydrogen and intrinsic point defects in olivine. *Z. Phys. Chem.* 207, 147–162.
- Kohlstedt, D.L., Mackwell, S.J., 1999. Solubility and diffusion of “water” in silicate minerals. In: Wright, K., Catlow, R. (Eds.), *Microscopic Properties and Processes in Minerals*. *Kluwer Academic Publishers*, pp. 539–559.
- Kohlstedt, D.L., Keppler, H., Rubie, D.C., 1996. Solubility of water in the alpha, beta and gamma phases of (MgFe)(2)SiO<sub>4</sub>. *Contrib. Min. Petrol.* 123, 345–357.
- Kohn, S.C., 2006. Structural studies of OH in nominally anhydrous minerals using NMR. In: Keppler, H., Smyth, J.R. (Eds.), *Water in Nominally Anhydrous Minerals*. *Rev. Min. Geochem.* 62, 53–66.
- Kröger, F.A., Vink, H.J., 1965. Relation between the concentrations of imperfections in crystalline solids. In: Steiz, F., Turnbull, D. (Eds.), *Solid State Phys.* 3, 307–435.
- Kurosawa, M., Yurimoto, H., Sueno, S., 1997. Patterns in the hydrogen and trace element compositions of mantle olivines. *Phys. Chem. Min.* 24, 385–395.

- Lemaire, C., Kohn, S.C., Brooker, R.A., 2004. The effect of silica activity on the incorporation mechanisms of water in synthetic forsterite: a polarised infrared spectroscopic study. *Contrib. Min. Petrol.* 147, 48–57.
- Libowitzky, E., Rossman, G.R., 1996. Principles of quantitative absorbance measurements in anisotropic crystals. *Phys. Chem. Min.* 23, 319–327.
- Lithgow-Bertelloni, C., Richards, M.A., 1995. Cenozoic plate driving forces. *Geophys. Res. Lett.* 22, 1317–1320.
- Mackwell, S.J., Kohlstedt, D.L., Paterson, M.S., 1985. The role of water in the deformation of olivine single crystals. *J. Geophys. Res.* 90, 11319–11333.
- Mackwell, S.J., Dimos, D., Kohlstedt, D.L., 1988. Transient creep of olivine—point defect relaxation times. *Phil. Mag.* 57, 779–789.
- Mackwell, S.J., Kohlstedt, D.L., 1990. Diffusion of hydrogen in olivine—implications for water in the mantle. *J. Geophys. Res.* 95, 5079–5088.
- Mao, H.K., Bell, P.M., England, J.L., 1971. Tensional errors and drift of the thermocouple electromotive force in the single-stage piston-cylinder apparatus. *Carnegie Inst. Wash. Year Book* 70, 281–287.
- Matveev, S., O'Neill, H.S., Ballhaus, C., Taylor, W.R., Green, D.H., 2001. Effect of silica activity on OH-IR spectra of olivine: Implications for low- $\alpha$ SiO<sub>2</sub> mantle metasomatism. *J. Petrol.* 42, 721–729.
- Mei, S., Kohlstedt, D.L., 2000. Influence of water on plastic deformation of olivine aggregates. 2. Dislocation creep regime. *J. Geophys. Res.* 105, 21471–21481.
- Miller, G.H., Rossman, G.R., Harlow, G.E., 1987. The natural occurrence of hydroxide in olivine. *Phys. Chem. Min.* 14, 461–472.
- Misener, D.J., 1974. Cationic diffusion in olivine to 1400°C and 35 kbar. In: Hofmann, A.W., Giletti, B.J., Yoder Jr., H.S., Yund, R.A. (Eds.), *Geochemical and Transport Kinetics*. Carnegie Institution of Washington, pp. 117–138.
- Mosenfelder, J.L., Deligne, N.I., Asimow, P.D., Rossman, G.R., 2006. Hydrogen incorporation in olivine from 2–12 GPa. *Am. Min.* 91, 285–294.
- Nabarro, F.R.N., 1967. Steady-state diffusional creep. *Phil. Mag.* 16, 231–237.
- Nakamura, A., Schmalzried, H., 1983. On the nonstoichiometry and point-defects of olivine. *Phys. Chem. Min.* 10, 27–37.
- Nix, W.D., Gascaner, R., Hirth, J.P., 1971. Contribution to theory of dislocation climb. *Phil. Mag.* 23, 1339–1349.
- Paterson, M.S., 1982. The determination of hydroxyl by infrared-absorption in quartz, silicate-glasses and similar materials. *Bull. Min.* 105, 20–29.
- Pawley, A.R., Wood, B.J., 1995. The high-pressure stability of talc and 10 Å phase: potential storage sites for H<sub>2</sub>O in subduction zones. *Am. Min.* 80, 998–1003.
- Pichavant, M., Mysen, B.O., Macdonald, R., 2002. Source and H<sub>2</sub>O content of high-MgO magmas in island arc settings: an experimental study of a primitive calc-alkaline basalt from St. Vincent Lesser Antilles arc. *Geochim. Cosmochim. Acta* 66, 2193–2209.
- Pitzer, K.S., Sterner, S.M., 1994. Equations of state valid continuously from zero to extreme pressures for H<sub>2</sub>O and CO<sub>2</sub>. *J. Chem. Phys.* 101, 3111–3116.
- Regenauer-Lieb, K., 2006. Water and geodynamics. In: Keppler, H., Smyth, J.R. (Eds.), *Water in Nominally Anhydrous Minerals*. *Rev. Min. Geochem.* 62, 451–474.
- Robie, R.A., Hemingway, B.S., 1995. Thermodynamic properties of minerals and related substances at 298.15 K and 1 bar (10<sup>5</sup> Pascals) pressure and at higher temperatures. *U.S. Geol. Surv. Bull.* 2131, 461.
- Ruoff, A.L., 1965. Mass transfer problems in ionic crystals with charge neutrality. *J. Appl. Phys.* 36, 2903–2907.
- Ryerson, F.J., Durham, W.B., Cherniak, D.J., Lanford, W.A., 1989. Oxygen diffusion in olivine—effect of oxygen fugacity and implications for creep. *J. Geophys. Res.* 94, 4105–4118.
- Schmalzried, H., 1974. *Solid State Reactions*. Verlag Chemie, Weinheim, 214 pp.
- Smyth, D.M., Stocker, R.L., 1975. Point defects and non-stoichiometry in forsterite. *Phys. Earth Planet. Int.* 10, 183–192.
- Stocker, R.L., Smyth, D.M., 1978. Effect of enstatite activity and oxygen partial pressure on the point-defect chemistry of olivine. *Phys. Earth Planet. Int.* 16, 145–156.
- Tingle, T.N., 1988. Retrieval of uncracked single-crystals from high-pressure in piston-cylinder apparatus. *Am. Min.* 73, 1195–1197.
- Tsai, T.L., Dieckmann, R., 2002. Variation of the oxygen content and point defects in olivines, (Fe<sub>x</sub>Mg<sub>1-x</sub>)<sub>2</sub>SiO<sub>4</sub> 0.2=x=1.0. *Phys. Chem. Min.* 29, 680–694.
- Walker, A.M., Wright, K., Slater, B., 2003. A computational study of oxygen diffusion in olivine. *Phys. Chem. Min.* 30, 536–545.
- Wanamaker, B.J., 1994. Point-defect diffusivities in San Carlos Olivine derived from reequilibration of electrical-conductivity following changes in oxygen fugacity. *Geophys. Res. Lett.* 21, 21–24.
- Wang, D.J., Mookherjee, M., Xu, Y.S., Karato, S., 2006. The effect of water on the electrical conductivity of olivine. *Nature* 443, 977–980.
- Wang, Z.Y., Hiraga, T., Kohlstedt, D.L., 2004. Effect of H<sup>+</sup> on Fe–Mg interdiffusion in olivine, (FeMg)<sub>2</sub>SiO<sub>4</sub>. *Appl. Phys. Lett.* 85, 209–211.
- Watson, E.B., Wark, D.A., Price, J.D., Van Orman, J.A., 2002. Mapping the thermal structure of solid-media pressure assemblies. *Contrib. Min. Petrol.* 142, 640–652.
- Weertman, J., 1999. Microstructural mechanisms of creep. In: Meyers, M.A., Armstrong, R.W., Kirschner, H. (Eds.), *Mechanics and Materials: Fundamentals and Linkages*. John Wiley & Sons, pp. 451–488.
- Wright, K., 2006. Atomistic models of OH defects in nominally anhydrous minerals. In: Keppler, H., Smyth, J.R. (Eds.), *Water in Nominally Anhydrous Minerals*. *Rev. Min. Geochem.* 62, 67–83.
- Yoshino, T., Matsuzaki, T., Yamashita, S., Katsura, T., 2006. Hydrous olivine unable to account for conductivity anomaly at the top of the asthenosphere. *Nature* 443, 973–976.
- Zhao, Y.H., Ginsberg, S.B., Kohlstedt, D.L., 2004. Solubility of hydrogen in olivine: dependence on temperature and iron content. *Contrib. Min. Petrol.* 147, 155–161.